Mmp14 is required for matrisome homeostasis and circadian rhythm in fibroblasts

Ching-Yan Chloé Yeung[1$]*, Richa Garva[1$], Adam Pickard[1], Yinhui Lu[1], Venkatesh Mallikarjun[1], Joe Swift[1], Susan H. Taylor[1], Jyoti Rai[2], David R. Eyre[2], Mayank Chaturvedi[3], Yoshifumi Itoh[3], Qing-Jun Meng[1], Cornelia Mauch[4], Paola Zigrino[4], and Karl E. Kadler[1]*

[1] Wellcome Centre for Cell-Matrix Research, Faculty of Biology, Medicine & Health, University of Manchester, Manchester Academic Health Science Centre, Manchester, M13 9PT UK.

[2] Department of Orthopedics, University of Washington, Seattle, WA, USA.

[3] Kennedy Institute of Rheumatology, University of Oxford, Oxford, UK.

[4] Department of Dermatology and Venereology, University of Cologne, Faculty of Medicine and University Hospital Cologne, 50937 Cologne, Germany.

C-YCY current address: Institute of Sports Medicine Copenhagen, Department of Orthopedic Surgery, Copenhagen University Hospital – Bispebjerg and Frederiksberg, Copenhagen, Denmark, and Center for Healthy Aging, Department of Clinical Medicine, University of Copenhagen, Denmark.

[$] Authors contributed equally.

* Co-corresponding authors.

Running title: Inter-dependence of matrix homeostasis and the circadian clock

Keywords: cell surface enzyme, circadian rhythm, collagen, connective tissue, CRISPR/Cas-9, electron microscopy, gene knockout, matrix metalloproteinase (MMP), protein self-assembly, tendon.

ABSTRACT

The circadian clock in tendon regulates the daily rhythmic synthesis of collagen-I and the appearance and disappearance of small-diameter collagen fibrils in the extracellular matrix. How the fibrils are assembled and removed is not fully understood. Here, we first showed that the collagenase, membrane type I-matrix metalloproteinase (MT1-MMP, encoded by *Mmp14*), is regulated by the circadian clock in postnatal mouse tendon. Next, we generated tamoxifen-induced *Col1a2-Cre-ERT2::Mmp14* KO mice (*Mmp14* conditional knockout (CKO)). The CKO mice

developed hind limb dorsiflexion and thickened tendons, which accumulated narrow-diameter collagen fibrils causing ultrastructural disorganization. Mass spectrometry of control tendons identified 1195 proteins of which 212 showed time-dependent abundance. In *Mmp14* CKO mice 19 proteins had reversed temporal abundance and 176 proteins lost time dependency. Among these, the collagen crosslinking enzymes lysyl oxidase-like 1 (LOXL1) and lysyl hydroxylase 1 (LH1; encoded by *Plod2*) were elevated and had lost time-dependent regulation. High-pressure chromatography confirmed elevated levels of hydroxylysine aldehyde (pyridinoline) crosslinking of collagen in CKO tendons. As a result, collagen-I was refractory to extraction. We also showed that CRISPR-Cas9 deletion of *Mmp14* from cultured fibroblasts resulted in loss of circadian clock rhythmicity of period 2 (PER2), and recombinant MT1-MMP was highly effective at cleaving soluble collagen-I but less effective at cleaving collagen pre-assembled into fibrils. In conclusion, our study shows that circadian clock-regulated *Mmp14* controls the rhythmic synthesis of small diameter collagen fibrils, regulates collagen crosslinking, and its absence disrupts the circadian clock and matrisome in tendon fibroblasts.

INTRODUCTION

Tendon development in mice is apparent from embryonic day 14.5 when narrow (~ 50 nm diameter) collagen fibrils begin to appear in channels between embryonic fibroblasts [1]. The fibrils increase in number during embryonic development and remain attached to fibripositors at the cell surface. At birth, fibripositors disappear, and the fibrils detach from cells and increase in diameter [2]. Thus, at the ultrastructural level, tendon development can be defined by stage 1 (embryonic) characterized by the presence of exclusively narrow fibrils, progressing to stage 2 shortly after birth when the fibril diameter distribution is multimodal (mean diameters of ~ 50 nm, ~150 nm and ~250 nm). Mice lacking *Mmp14* (encodes MT1-MMP) are morphologically normal at birth but later exhibit reduced size and several abnormalities, and die within a few weeks of birth[3, 4]. Electron microscopy shows that detachment of the narrow fibrils from the cells and subsequent increase in fibril diameter do not occur in *Mmp14*-deficient neonatal mice [2]; thus, tendon development arrests at the end of stage 1. A motivation for the present study was to determine the role of MT1-MMP in adult tendon ECM homeostasis. Of particular interest to the present study, the narrow fibrils in postnatal tendon are under the control of the circadian clock [5].

MT1-MMP is a transmembrane matrix metalloproteinase first identified for its ability to activate progelatinase A (proMMP2) and thereby enhance cellular invasion of reconstituted

basement membrane [6]. Extensive studies have showed that it can cleave a wide range of cellular and extracellular substrates including protease inhibitors, chemokines, cytokines, cell receptors, proMMP13, fibronectin and collagens (see [7]). Therefore, aberrant *Mmp14* expression may result in major disruptive effects on matrix homeostasis. In humans, *Mmp14* has been implicated in cancer cell invasion [8, 9], which has been attributed to its ability to degrade extracellular matrix (ECM) macromolecules, especially type I collagen (collagen-I) [10-12]. Like other vertebrate collagenases, MT1-MMP cleaves members of the fibrillar collagen family at the characteristic ¾-¼ site between residues 775 and 776 in each collagen α-chain [13]. MT1-MMP is distinct from other MMPs in that its deletion in mice results in early postnatal death [3, 4]. The mice fail to thrive and exhibit a wide range of pathologies in addition to walking difficulties including defective osteogenesis and angiogenesis [3, 4, 14], altered white adipose tissue [15] and modulation of inflammatory responses [16], activation of transforming growth factor β1 (TGFb1) [17], and deregulation of α5β1 integrin endocytosis [18].

We noted that the organ systems affected in the *Mmp14*-null mouse overlap with those affected in mice that lack a functional circadian clock. These include, bone formation [19], adipogenesis [20], inflammatory immune responses [21], and angiogenesis [22]. Furthermore, as noted above, the narrow fibrils in postnatal mouse tendon are under circadian clock control. Circadian clocks are cell-autonomous time keeping mechanisms that optimize cellular activities in anticipation of varying time-of-day demands on the cell [23, 24]. The molecular pacemaker is a transcription-translation feedback loop that is driven by two transcription activators, BMAL1 (bone and muscle Arnt-like 1) and CLOCK (circadian locomotor output cycles kaput protein), and two transcription repressors, CRY (cryptochrome) and PER (period) that inhibit the transcriptional complex[25]. A search of public databases showed that *Mmp14* transcripts are under circadian clock control in mouse suprachiasmatic nucleus (the central pacemaker located in the anterior hypothalamus), lung, heart, cartilage, and adipose tissue [26]. Time-series transcriptomic profiling of mouse tendon (ArrayExpress accession no. E-MTAB-7743 [27]) showed circadian expression of the *Mmp14* transcript. However, the biological role of a circadian-regulated matrix metalloproteinase in adult tendons is not fully understood.

Here we generated a type I collagen-specific conditional *Mmp14* knockout (CKO) mouse ($Col1a2^{CreERT2}$::$Mmp14^{F/F}$) and performed electron microscopy, proteomics, collagen content, and crosslink analyses of tendon. Our results show a circadian control of MT1-MMP in tendon and

93 identify new functions for *Mmp14* in maintaining a functional circadian clock in fibroblasts, in
94 matrix homeostasis, and in ensuring normal crosslinking of collagen fibrils, in tendon.

95

96 **RESULTS**

97 ***Levels of Mmp14* and MT1-MMP are circadian in postnatal mouse tendon.** The readouts from 3
98 independent microarray probe sets showed the highest expression of *Mmp14* at the night-day
99 transition (**Fig. S1A**, data replotted from data published by Yeung *et al.* 2014 [27]). Time-series
100 western blot analysis showed peak levels of MT1-MMP at circadian time 3 (CT3; 3 h into the day),
101 which was approximately 4 hours after the peak in transcript levels (**Fig. S1B**). Next, we showed
102 that time-of-day-dependent expression of *Mmp14* observed in mouse Achilles and tail tendons
103 was abolished in tendons from tendon-specific *Bmal1* knockout *(Scx-Cre::Bmal1*$^{F/F}$) and global
104 *Clock*-null (*ClockΔ19*) mice which lack circadian rhythms in their tendons [5, 27]. We did this by
105 examining relative *Mmp14* mRNA levels in tendons at two time points based on the peak and
106 nadir *Mmp14* expression and MT1-MMP levels in mouse tendon: zeitgeber time 3 (ZT3; 3 h into an
107 external or environmental cue, and in this case it was light of a 12-h light/12-h dark cycle) and
108 ZT15 (3 h into the dark phase) (**Fig. S1C-E**). As such, the rhythmic expression of *Mmp14* depends
109 on an intact local circadian clock in tendon tissues.

110

111 **Accumulation of narrow-diameter collagen fibrils in tendons with a postnatal deletion of**
112 ***Mmp14*.** Because global knockout of *Mmp14* results in perinatal death and the tendon-specific
113 *Mmp14* knockout mouse (*Scx-Cre::Mmp14*$^{F/F}$) does not progress past stage 1 tendon development
114 [2], we generated the conditional collagen-I-specific *Mmp14* knockout mouse
115 (*Col1a2*^{CreERT2}*::Mmp14*$^{F/F}$, abbreviated to *Mmp14* CKO or CKO), which was inducible by tamoxifen
116 [28]. We treated 4 week-old *Col1a2*^{CreERT2}*::Mmp14*$^{F/F}$ (abbreviated to *Mmp14* CKO or CKO) mice (time
117 point 0, T0) with tamoxifen for 5 weeks to induce deletion of *Mmp14* in all cells expressing *Col1a2*
118 (i.e., mainly fibroblasts including tenocytes) and harvested tendons at 10-, 14-, 18- and 22-weeks
119 of age (T1, T2, T3 and T4, respectively; see schematic in **Fig. 1A**). We noticed that tamoxifen-
120 treated mice had difficulty walking, severe skin thickening[28] and dorsiflexion of the hind limbs (**Fig.**
121 **1B**). Examination of the tails showed thickening of tendon bundles (**Fig. 1C**). Q-PCR analysis of
122 *Mmp14* expression in tendons at ZT3 and ZT15 showed time-dependent expression of *Mmp14* in
123 wildtype (WT) mice but was almost undetected in tamoxifen-treated mice (**Fig. 1D**). Western blot
124 analysis established there was an absence of MT1-MMP in primary fibroblasts isolated from

125 *Mmp14* CKO tendons (**Fig. 1E**). Transmission electron microscopy analysis showed a progressive
126 increase in the abundance of narrow-diameter (~ 50 nm) collagen fibrils during T1 to T4 in CKO
127 tendons compared to controls (**Fig. 1F, G** and **Fig. S2**). In T4 CKO tendons narrow fibrils were also
128 observed within fibricarriers (**Fig. S2B**). We also noted a gradual increase in irregular fibril cross
129 sections from T0 to T4 in CKO tendons (**Fig. 1H**). Serial block face-scanning electron microscopy,
130 using established methods [29], showed gross disruption of the collagen fibril network in CKO
131 tendons compared to tendons of littermates not treated with tamoxifen (**Fig. 1I, J** and **Movie 1**
132 and **Movie 2**). During dissection we noticed that CKO tendons were brittle and would break easily.
133 Therefore, samples were not analyzed by mechanical testing. These data confirm that *Mmp14* is
134 necessary for postnatal tendon tissue homeostasis.

135

136 **Altered temporal patterns of abundance of soluble proteins in *Mmp14* CKO tendons.** To
137 understand the consequences of *Mmp14* deficiency on time dependent expression of proteins *in*
138 *vivo* we performed proteomics analysis of tendon harvested at two time points in the 24-hour day
139 from *Mmp14* CKO mice and control littermates (**Fig. 2A**). Note that, severe walking difficulties in
140 *Col1a2-Cre-ERT2::Mmp14*$^{F/F}$ mice treated with tamoxifen meant that insufficient numbers of mice
141 were available for a circadian time series collection of tissues every 4 hours over two days as
142 performed previously for studies of the tendon circadian clock [5]. Instead, two time points, ZT3 and
143 ZT15 were selected (**Fig. S1A** and **B**). T2 (5 weeks post tamoxifen treatment) was chosen because it
144 was the time point where a more prominent fibrotic phenotype was detected in skin[28] and
145 tendons, deletion of *Mmp14* was complete, and it was still possible to dissect CKO tendons cleanly
146 from the limb [28]. We extracted non-covalently bound proteins with sodium laurate-sodium
147 deoxycholate (SL-DOC) buffer using methods previously described [5]. Analysis of samples identified
148 1195 proteins with ≥ 2 peptides per protein of which 212 showed time-dependent abundance, as
149 shown by MetaCycle analysis, with good reproducibility between biological replicates as indicated
150 by Pearson analysis across consecutive 24-hour periods (**Fig. S3A** and **Table S1 and Table S2**).
151 Comparing logged ZT15/ZT3 fold changes for 1195 proteins showed that the absence of *Mmp14* in
152 CKO tendons disrupted time-dependent protein abundances (**Fig. S3B**). Of the 212 time-
153 dependent proteins detected in control tendons, 17 remained time-dependent and have a
154 statistically significant (FDR adjusted p-value <0.05) difference in expression between the two time
155 points in CKO tendons, 19 proteins exhibited a reversed time-dependent expression pattern (**Fig.**
156 **2B**), and 176 had lost time-dependent abundance pattern in CKO tissues (**Fig. 2C**). A search

157 through the previously published rhythmic soluble mouse tail tendon proteome (see [5]) revealed
158 27 common proteins amongst the 176 that had lost temporal abundance. Interaction analysis of
159 these 27 proteins that have lost circadian rhythmic abundancy revealed direct interactions
160 between fibronectin (FN1), the MT1-MMP substrate accumulated in *Mmp14*-deficient mice [2], and
161 19 out of 22 of the proteins recognized by Pathway Commons (**Fig. 2D**). Together, these data
162 demonstrate that deletion of *Mmp14* in postnatal fibroblasts disrupts time-dependent abundance
163 of soluble proteins, including those that have circadian rhythmicity, in tendon tissue.

164

165 **Dysregulation of the tendon matrisome and elevated crosslinking in the absence of *Mmp14.***
166 Since *Mmp14* CKO tendons exhibit gross ultrastructural changes in the ECM an investigation of
167 matrisome proteins was extended to proteins that did not have time dependent abundance. We
168 found that 121 matrisome proteins had differential abundances in CKO tendons compared to
169 control tendons (i.e., 62 proteins higher and 59 proteins lower abundance in CKO tendons; **Fig. 3**).
170 Interactions analysis revealed the direct and indirect effects of *Mmp14* deletion on and via
171 substrates and binding partners (**Fig. S4**). For example, there is increased abundance of the MT1-
172 MMP14 substrate proMMP2, which may have caused the modulated abundances of fibronectin,
173 cathepsin K (CTSK, which is circadian clock regulated and involved in collagen turnover), collagen V
174 (COL5A1), collagen VI (COL6A1, COL6A2), collagen XIV (COL14A1), collectin-12 (COLEC12), galectin
175 3 (LGALS3), tenascin C (TNC), tissue inhibitor of metalloproteinase 2 (TIMP2), and thrombospondin
176 2 (THBS2). Not all proteins were increased in abundance, e.g., there were reductions in COL2A1,
177 COL6A2, COL6A3, and decorin (DCN). Of particular interest, enzymes that catalyze
178 posttranslational modifications in collagen leading to crosslink formation were elevated and
179 included lysyl hydroxylase 2 (also known as procollagen-lysine, 2-oxoglutarate 5-dioxygenase 2
180 (PLOD2)) (up 13-fold), and lysyl oxidase-like 1 (LOXL1) (up 20-fold).

181 There was clear discrepancy between the accumulation of collagen fibrils in the *Mmp14*
182 CKO mice (see **Fig. S2B**) and the low levels of collagen-I detected by mass spectrometry of CKO
183 tissues (**Table S1** and **Fig. S4C**). Therefore, we collected tendons from T2 *Mmp14* CKO and control
184 mice at ZT3 and ZT15 and performed hydroxyproline analysis to quantify collagen. We also
185 subjected tendons to extraction in SL-DOC buffer, followed by hydroxyproline quantification.
186 Analysis of whole tissue and SL-DOC extracts showed ~98%:2% split between crosslinked collagen
187 in whole tissue and soluble collagen in the SL-DOC extract (**Table 1**). There was an increase of ~
188 6.4% in overall collagen content in CKO tendons, which was largely the result of collagen

189 accumulated at ZT15. However, there was ~8-fold increase in the amount of hydroxylysine
190 aldehyde in *Mmp14* CKO compared to control tendons at both time points (**Table 1**). Mass
191 spectrometry ruled out significant amounts of collagen-III as the source of hydroxylysine aldehyde
192 in the CKO samples. Therefore, the discrepancy in the number of collagen-I peptides extracted
193 into SL-DOC buffer, and the marked accumulation of collagen fibrils in the CKO tendons, was the
194 result of accumulation of collagen at ZT15 and decreased extractability because of increased
195 hydroxylysine aldehyde cross-linking of collagen-I [30] in the CKO tissues.

196

197 **Elevated *Pitx2* and PITX2 nuclear localization in *Mmp14* knockout cells.** To understand how loss
198 of *Mmp14* led to extensive crosslinking, we investigated a possible relationship between *Mmp14*
199 and paired-like homeodomain transcription factor 2 (PITX2), which is a transcription factor that
200 has been reported to regulate the expression of *Plod2* [31, 32], as well as collagen I and V [33]. We
201 showed by Q-PCR that levels of *Pitx2* mRNA are low in murine tail tendon at both ZT3 and ZT15
202 but markedly elevated in the CKO tendons (**Fig. 4A**). *Plod2* expression was also elevated ~10 fold in
203 CKO tendons (**Fig. 4B**). Next, we expressed PITX2-GFP in immortalized tail tendon fibroblasts
204 (iTTFs). Over-expression of PITX2-GFP was confirmed by Q-PCR (**Fig. 4C**), and although it was not
205 as pronounced as in *Mmp14* CKO tendons, resulted in a 2-fold increase in expression of *Plod2* (**Fig.**
206 **4D**), confirming that PITX2 drives the expression of *Plod2* in tendon fibroblasts. PITX2-GFP was
207 localized to cell nuclei (**Fig. 4E**) and this nuclear localization was enhanced in *Mmp14*-depeleted
208 fibroblasts (**Fig. 4F**). Over-expression of mCherry-MT1-MMP in PITX2-GFP expressing iTTFs
209 reversed the induced *Pitx2* and *Plod2* expression and enhanced *Col1a1* expression (**Fig. 4G-J**).
210 Together, these data show that *Mmp14* negatively regulates *Plod2* expression via PITX2.

211

212 **MT1-MMP-mediated cleavage of collagen-I is dispensable for postnatal tendon development.**
213 The amassing of narrow collagen fibrils in the CKO tendons prompted us to investigate if their
214 accumulation was a direct result of the absence of collagen fibril turnover in the absence of MT1-
215 MMP. Thus, we released intact collagen fibrils from 6-week-old mouse Achilles tendon and
216 examined the diameters before and after incubation of the fibrils with recombinant soluble MT1-
217 MMP (rMT1-MMP), which was synthesized as previously described [34]. The fibril diameters were
218 derived from mass-per-length measurements using scanning transmission electron microscopy [35].
219 The results showed no differences in fibril diameters between rMT1-MMP treated and untreated
220 samples (**Fig. 5A**). When assembled into fibrils, many of the collagen molecules are buried in the

221 core of the fibril and thereby inaccessible to MT1-MMP. Therefore, we incubated fibrils that had
222 been released from tendon overnight at 37 °C (to keep the fibrils intact) and 30 °C (to partially
223 depolymerize the fibrils), and then added rMT1-MMP to the suspension of fibrils. In control
224 experiments we incubated MT1-MMP with soluble collagen-I (i.e., not assembled into fibrils) in
225 the presence and absence of EDTA, which chelates Ca2+ ions and inactivates MT1-MMP (**Fig. 5B**).
226 SDS-PAGE and mass spectrometry were used to detect cleavage products. Liquid chromatography
227 with tandem mass spectrometry (LC-MS/MS) analysis of the cleavage products showed the
228 presence of a semi-tryptic peptide from the ¾ α1(I) fragment corresponding to the expected ¾-¼
229 cleave site, which confirmed that rMT1-MMP had cleaved soluble collagen-I molecules at the
230 expected Gly775 and Ile776 site (**Fig. 5C** and **D**). However, incubation of rMT1-MMP with the
231 suspension of fibrils resulted in only a small proportion of the collagen being cleaved and only
232 when the reaction was performed overnight at 30 °C (**Fig. 5B**, white box). The most likely
233 explanation was partial depolymerization of the fibrils at this temperature, resulting in release of
234 collagen molecules that were then susceptible to cleavage by rMT1-MMP. As expected, cleavage
235 was inhibited by EDTA. We noticed a downward shift in mobility of β-chains (crosslinked α-chains),
236 which was not inhibited by EDTA. It is likely, therefore, that this was the result of non-MMP
237 activity in the collagen fibril preparation (**Fig. 5B**). These results showed that collagen is largely
238 protected from cleavage by MT1-MMP when it is assembled into fibrils.

239 To investigate further the contribution of the collagen-I ¾-¼ cleavage site to collagen fibril
240 homeostasis, we used transmission electron microscopy to examine tendons from the *Col-r/r*
241 mouse, which carries a targeted mutation in *Col1a1* [36] that renders both the α1(I) and α2(I) chains
242 resistant to cleavage by MMPs at the ¾-¼ site [37] (**Fig. S5A**). The results show that 23-week-old
243 (equivalent to T4 *Mmp14* CKO mice) *Col-r/r* mouse tendons exhibit a broad distribution of collagen
244 fibril diameters, in contrast to what was observed in the CKO mice (compare **Fig. 5B-E**). These
245 observations showed that the accumulation of narrow fibrils in the postnatal CKO mice is not fully
246 explained by the lack of cleavage of the ¾-¼ site in collagen-I.

247

248 **Deletion of *Mmp14* dampens the PER2::Luc circadian rhythm amplitude in cultured tendon**
249 **fibroblasts.** The occurrence of increased numbers of narrow fibrils and increased irregular fibril
250 profiles were reminiscent of tendons with a disrupted circadian rhythm [5]. To determine if *Mmp14*
251 deletion affects the endogenous circadian clock, we used iTTFs from the circadian reporter
252 PER2::Luc mouse (iTTF-PER2::Luc or abbreviated to 'iTTFs'), which enabled us to monitor the

253 circadian rhythm in real time [5]. In initial experiments we incubated clock synchronized iTTF cells
254 with the broad spectrum MMP inhibitor GM6001, which markedly reduced the amplitude of the
255 circadian rhythm in treated cells compared to untreated controls (**Fig. S6A, B**). Next, we
256 performed siRNA knockdown of *Mmp14.* Q-PCR showed that knockdown was highly effective at
257 reducing the expression of *Mmp14* (**Fig. S6C**) and bioluminescence showed that the circadian clock
258 rhythm was dampened in *siMmp14* treated cells (**Fig. S6D**). Next, we performed clustered
259 regularly interspaced short palindromic repeats (CRISPR) and CRISPR-associated protein 9 (Cas9)
260 mediated knockout of *Mmp14* in iTTFs (**Fig. S6E**). Western blot analysis using an anti-MT1-MMP
261 antibody showed absence of MT1-MMP in 7 different clones (**Fig. S6F**). *Mmp14*-null iTTF clones
262 were unable to sustain a circadian rhythm in response to dexamethasone (**Fig. 6A**). Restoring
263 *Mmp14* expression alone via lentiviral transduction rescued robust circadian oscillations (**Fig. 6B,**
264 **C**). Together these data show that in mouse tendon tissue *Mmp14* expression is required for a
265 robust circadian rhythm in tendon fibroblasts.

266

267 **Discussion**

268 This study has shown that *Mmp14* is a master mediator of ECM homeostasis in adult tendons, as
269 shown by the accumulation of small-diameter collagen fibrils and major changes in the matrisome
270 when MT1-MMP is absent. We suggest that accumulation of the narrow collagen fibrils is the
271 result of the accumulation of MT1-MMP substrates as well as loss of robust circadian rhythm,
272 widespread changes to the ECM proteome, and elevated collagen crosslinking. Based on these
273 findings we propose that a bi-directional dependency exists between matrix homeostasis and the
274 circadian clock.

275 The lead observation for this study was the circadian expression of *Mmp14*. The peak of
276 *Mmp14* expression in murine tendon is at CT3, which is in good agreement with the peak of *Bmal1*
277 expression [27]. Circadian clock regulated genes usually contain one or more transcriptional
278 elements, RORE, DBPE and E-box [38]. Noteworthy, a CACGTT (E-box) sequence is located 1.6 kb
279 upstream of the translational start site of murine and human *Mmp14,* which would facilitate
280 rhythmic binding of CLOCK-BMAL1 to E-box motifs [39]. *Mmp14* gene expression has been shown to
281 be rhythmically expressed in murine lung, heart, kidney and adipose as well as the
282 suprachiasmatic nucleus [40]. Therefore, it is likely that *Mmp14* is a BMAL1 responsive gene and its
283 expression is restricted to a specific time of day across organ systems. We confirmed at the
284 protein level that MT1-MMP is under circadian clock control in tendon, which was in line with

285 circadian rhythmic levels of MT1-MMP and MMP2 activation observed in murine tendon
286 fibroblasts [41]. The peak of abundance of MT1-MMP was particularly narrow (~ 4 hours after the
287 peak of *Mmp14*) (**Fig. 1**), which is consistent with observations that MT1-MMP has a fast turnover
288 of 4.8 h, and puts MT1-MMP in the top 1% of rapidly turned-over proteins in the proteome [42, 43].
289 Together, these results and those of others studying organs other than tendon, show that *Mmp14*
290 is under the control of the circadian clock which results in the synthesis of MT1-MMP in the
291 morning. The appearance of MT1-MMP at CT3-7 coincides with the rhythmic abundance of
292 collagen-I and with the onset of collagen fibril formation, in tendon [5], suggesting that *Mmp14* is
293 important for collagen fibril formation.

294 Previously, a *Scx-Cre* driver was used to delete *Mmp14* in embryonic tendons [2] because
295 *scleraxis* is expressed by all tendon progenitors [44] . *Scx-Cre::Mmp14*$^{F/F}$ neonatal tendons were
296 thinner because the potential fibronectin 'molecular bridge' between the cell surface and
297 collagen-I fibrils cannot be cleaved by MT1-MMP. So there is an overall reduction in fibrils
298 assembled in the ECM, perhaps limited to cell size and/or fibril nucleation sites on the cell surface
299 [45], contributing to the smaller tendon width [2]. The use of an inducible *Scx-Cre* in postnatal tendons
300 would not yield a complete *Mmp14* deletion because *scleraxis* expression in tendon becomes
301 limited to the epitenon by 3 months of age [46]. The major cell type in postnatal mouse tendons is
302 the fibroblast and single cell transcriptomics experiments performed on healthy adult mouse
303 Achilles tendons have confirmed that *Col1a2* expression is limited to fibroblast [47]. Therefore, a
304 tamoxifen-inducible *Col1a2-Cre* was chosen to drive the deletion of *Mmp14* in postnatal tendons.
305 In contrast to thinner neonatal tendons resulting from embryonic *Mmp14* deletion, postnatal
306 *Mmp14* deletion is initiated at 5 weeks of age, well into stage 2 of tendon development when
307 collagen-I fibrils are released from the cell surface and permitted to grow laterally [45] and when a
308 circadian rhythm is established in peripheral tissues in rodents (reviewed by [48]). The consequence
309 is tendon thickening, resulting from multiple factors: (1) halted turnover of fibronectin and
310 collagen V, which act as nucleators for collagen-I fibril assembly, (2) lack of removal of circadian-
311 regulated collagen-I that add onto existing large fibrils, (3) increased abundance of collagen
312 crosslink enzymes (via PITX2), which stabilize new narrow fibrils and collagen-I molecules on larger
313 fibrils, and (4) major disruption to the circadian rhythm and the temporally regulated matrisome,
314 including molecules known to regulate collagen fibrillogenesis (e.g., lumican, etc).

315 We showed that tamoxifen-induced deletion of *Mmp14* in postnatal mice resulted in a
316 severe tendon phenotype marked by dorsiflexion of hind limbs, tissue thickening, mistimed
317 expression of 195 proteins (including 18 matrisome proteins) and altered abundance of a 104

318 matrisome proteins. The relatively large number of proteins with altered abundance is in line with
319 ChIP and reporter vector studies showing that MT1-MMP regulates more than 100 genes [49]. Our
320 proteomics analysis of time-dependent abundance of proteins showed that MT1-MMP is a major
321 regulator of the matrisome in tendon. Proteins with elevated levels included fibronectin, collagens
322 I and V (which are major protagonists in fibril assembly in tendon), collagen XIV (its expression in
323 tendon is associated with collagen fibril assembly and growth [50, 51]), and prolyl 3-hydroxylase,
324 whose absence in mice leads to tendon abnormalities [52]. Fibronectin is a substrate for MT1-MMP;
325 therefore, its increase in abundance might be a direct result of the absence of *Mmp14*. However,
326 MMP3 (stromelysin-1), which can degrade fibronectin [53], was upregulated in CKO tendons. The
327 abundance of fibronectin might also be in response to injury or inflammatory signals caused by the
328 lack of *Mmp14*, which has been shown to put a brake on pro-inflammatory responses (reviewed
329 by [49]), perhaps by activating PI3/Akt3/GSK3 signaling [16]. Notably, lumican was upregulated
330 whereas the other small leucine rich proteoglycans, decorin, fibromodulin, keratocan, and lubricin,
331 were down regulated. Lumican is a collagen-binding proteoglycan [54] and was proposed to facilitate
332 interchain collagen crosslinking by interacting with collagen and lysyl oxidase (reviewed by [55]).
333 Lumican has a critical role in the organization of collagen fibrils in tendons and cornea and is
334 profibrotic in heart [56]. Furthermore, lumican knockout leads to reduced collagen crosslinking [57].
335 The increased levels of lumican were matched by the increase in levels of LOXL1 and LH2, which
336 post-translationally modify lysyl residues in collagen and lead to highly stable crosslinks, especially
337 in collagen-I. Taken together, these protein changes are in line with increased pyridinoline
338 crosslinks, which explains the low extractability of collagen-I from the CKO tendons.

339 We suggest that the circadian clock in *Mmp14*-null cells is 'stuck' at ZT15. Therefore,
340 proteins that would normally be expressed only at night are expressed day and night in CKO
341 tendons. This would explain the overabundance of pro-matrix proteins such as collagen-I,
342 collagen-V, collagen-XIV, lumican, fibronectin, LOXL1, and LH2, which are normally only expressed
343 at night but in the CKO tendons are expressed throughout 24 hours (see **Fig. 3**). The reasons why
344 the small diameter fibrils are attached to cell surfaces, perhaps via fibripositors, is unclear. One
345 explanation is that the processes of fibril turnover and internalization are arrested in CKO tendons.
346 The observation that collagen assembled into fibrils is mostly inaccessible to MT1-MMP might
347 suggest that fibril turnover is not the primary explanation. Alternatively, the accumulation of fibrils
348 might result from the inability of cells to release collagen fibrils from the cell surface. As previously
349 suggested, fibronectin might act as a molecular bridge between collagen and receptors at the cell
350 surface [2]. The appearance of a more normal collagen matrix in the *Col-r/r* mouse would also

351 suggest that lack of cleavage of collagen-I (at least at the ¾-¼ site) by MT1-MMP does not explain
352 the accumulation of narrow fibrils in CKO tendons. The persistence of collagen fibrils in the
353 absence of MT1-MMP may be partially explained by an increase in covalent crosslinks in collagen
354 (via LOXL1 and LH2, and promoted by lumican). Moreover, the increased availability of soluble
355 collagen-I, in the absence of MT1-MMP, would be expected to lead to an increase in the number
356 of collagen fibrils formed. Taken together, we propose that the accumulation of small diameter
357 collagen fibrils attached to surfaces of tendon resident cells in CKO tendons is likely to be the
358 consequence of compounding factors including the circadian clock being stuck at ZT15, wholesale
359 changes in the matrisome, lack of proteolytic cleavage of collagens, fibronectin and other
360 matrisome proteins, increased collagen crosslinking (making the fibrils refractory to disassociation
361 and turnover), increased synthesis of collagen-I and V, and failure of cells to release fibrils to the
362 matrix. In conclusion, we have demonstrated the pivotal and multifaceted role of *Mmp14* in
363 circadian clock biology, matrisome regulation, and collagen fibril formation, together with the
364 maturation of tendon fibroblasts during early postnatal growth that requires *Mmp14*. Our data
365 also highlight the interdependence of *Mmp14*-dependent matrix homeostasis and the circadian
366 clock.

367 Finally, our proteomics analysis identified additional changes in the proteome not directly
368 related to the matrisome (data shown in **Fig. 2C** and **Supplementary Data 2**). These included
369 changes to the cytoskeleton, which our current study could not distinguish between direct or
370 indirect consequences of the absence of *Mmp14*. It has been reported that the cytoplasmic and
371 transmembrane domains of MT1-MMP regulate non-proteolytic functions, including signal
372 transduction via the cytoplasmic tail activating ERK1/2 signaling independent of proteolysis [58, 59],
373 and gene regulation via a presumed nuclear localization signal in the transmembrane domain
374 (reviewed by [60]). MT1-MMP has a presumed nuclear localization signal [49, 61], and localizes to other
375 intracellular sites including caveolae, mitochondria, and the cytoskeleton to regulate calcium
376 levels leading to contractile dysfunction, and altered gene expression and ribosomal RNA
377 transcription (reviewed by [60]). It is possible that MT1-MMP has an intracellular scaffolding function
378 that regulates collagen fibril formation and matrix homeostasis.

379

380 **Acknowledgements**

381 The research was funded by Wellcome (110126/Z/15/Z and 203128/Z/16/Z) and the BBSRC
382 (BB/T001984/1) to KEK. CM and PZ were supported by Deutsche Forschungsgemeinschaft through

SFB 829 (Project-ID 73111208-SFB829 (B4)). VM was supported by a studentship from the Sir Richard Stapley Educational Trust. JS was funded by a Biotechnology and Biological Sciences Research Council (BBSRC) David Phillips Fellowship (BB/L024551/1). BC is supported by a Wellcome PhD studentship (210062/Z/17/Z). MC and YI was funded by Polish Ministry of Science & Higher Education (1291/MOB/IV/2015/0). Q-JM was supported by Medical Research Council project grants MR/T016744/1 and MR/P010709/1 and Versus Arthritis Senior Research Fellowship Award 20875. National Institutes of Health (NIH) Grant: (NIAMS) AR037318 to DRE. The authors would like to thank Ronen Schweitzer (Shriners Hospital for Children, Portland, OR, USA) for *Scx-Cre* mice, Jan Zamek, Alison Hallworth and Raymond Hodgkiss, and the University of Manchester Biological Support Facility for assistance in animal welfare and husbandry. Re-derivation of mouse strains and generation of expression vectors were performed by the Genome Editing Unit, University of Manchester. The proteomics was performed at the Biological Mass Spectrometry Facility in the Faculty of Biology, Medicine and Health (University of Manchester) with the assistance of Stacey Warwood and Ronan O'Cualain, and electron microscopy was performed in the Electron Microscopy Facility, Faculty of Biology, Medicine and Health (University of Manchester).

Author contributions:

Conceived the project and provided mechanistic insight: AP, C-YCY, KEK, RG.

Interpretation of results regarding the circadian clock: Q-JM.

Finalized the manuscript: C-YCY, KEK.

Designed and performed experiments and interpreted data: AP, C-YCY, DE, JR, MC, PZ, RG, ST.

Provided reagents: CM, PZ, YI.

Performed the electron microscopy: YL.

Performed bioinformatics analysis: JS, VM.

Competing Interests:

The authors declare no competing interests.

Table 1: Collagen content in control and *Mmp14* CKO tendons determined by hydroxyproline assay. N = 3. Values are mean ± SEM. Two-way ANOVA: *p=0.0146 for time effect, **p=0.0014 for genotype effect.

	Control		**CKO**	
	ZT3	ZT15	ZT3	ZT15
% hydroxyproline content per lyophilized whole tissue weight	70.97 ± 4.27	62.30 ± 5.25	71.43 ± 1.74	70.40 ± 6.35
% hydroxyproline content of SL-	1.50 ± 0.10	0.98 ± 0.31*	1.39 ± 0.12	0.81 ± 0.05*
Hydroxylysine aldehyde (pyridinoline) content per whole tissue hydroxyproline	0.009 ± 0.003	0.013 ± 0.002	0.095 ± 0.033**	0.095 ± 0.007**

418 **Figure legends**

419 **Figure 1. Accumulation of collagen fibrils in tendons from tamoxifen-induced conditional**
420 **deletion of *Mmp14* of *Col1a2CreERT2:Mmp14*$^{F/F}$ mice. A**, Schematic of *Mmp14* deletion in
421 fibroblasts of *Col1a2CreERT2:Mmp14*$^{F/F}$ (*Mmp14* CKO) mice *in vivo* by tamoxifen-chow feeding at 4
422 weeks of age for 5 weeks. Tissue was collected at T0 (before tamoxifen induction), T1, 2, 3 and 4
423 (1, 5, 9 and 13 weeks after tamoxifen induction, respectively). Control mice were not treated with
424 tamoxifen. **B-C**, Photographs showing thickening of skin of *Mmp14* CKO at site-matched locations
425 of the limb, and **C**, thickening of tendons in the tail compared to control litter mates at T4. **D,** Q-
426 PCR analysis for *Mmp14* at T4 control and CKO tendons at ZT3 and ZT15 (n=3). **E**, Western blotting
427 of MT1-MMP in fibroblasts isolated from control (Ctrl) and CKO Achilles tendons. Vinculin was
428 used as a protein loading control. **F,** Transmission electron microscopy analysis showed *Mmp14*
429 CKO tendons accumulated narrow diameter fibrils both in the ECM and inside cells (black arrows
430 and inset in T4 panel) but not in control tendons. **G**, Fibril diameter distributions of fibrils
431 measured in control and *Mmp14* CKO tendons at T4 show an increase in narrow-diameter (~50
432 nm) fibrils in *Mmp14* CKO tendons. **H**, Circularity of collagen fibril cross sections of *Mmp14* CKO
433 tendons showed significant irregularity compared to control fibrils at all time points after
434 tamoxifen induction, with increasing irregularity over time (270-470 fibrils measured per time
435 point; ****P<0.0001 for time, genotype and interaction). **I-J**, Single images selected from step-
436 through Movie 1 and Movie 2 generated from volume-EM analysis of control and CKO Achilles
437 tendons. Scale bar, 1 µm.

438

439 **Figure 2. Proteomic analysis of tendons from conditionally-deleted *Mmp14* mice. A**,
440 Experimental strategy and results summary of proteomics analysis of protein abundance in
441 tendons of *Col1a2CreERT2:Mmp14*$^{F/F}$ (CKO) compared to control littermates at ZT3, when *Mmp14*
442 levels are highest, and at 12 h apart (ZT15) (n=3). 1195 proteins were identified, 212 were
443 identified as significantly time-dependent in control tendons ($p<0.05$), of which 17 remained time-
444 dependent, 19 showed a statistical significant reversal of abundance pattern, and 176 were no
445 longer time-dependent in *Mmp14* CKO tendons. **B**, Heat map representation of proteins that
446 remained time-dependent in *Mmp14* CKO tendons, including proteins with abundance in anti-
447 phase to wild type tendons. **C**, Heat map representation of the abundance of 176 proteins that are
448 time-dependent in control tendons but are no longer time-dependent in *Mmp14* CKO tendons. **D**,
449 Interaction analysis of proteins that have lost circadian rhythmic abundancy in CKO tendons.

450

451 **Figure 3. Disruption of the soluble matrisome in CKO tendons.** Heatmap of Z-scored fold changes
452 for matrix proteins with differential abundance between control and CKO tendons (62 increased
453 abundance, 60 decreased abundance). Proteins are listed ranked by increasing abundance in
454 control tendons at ZT3.

455

456 **Figure 4. PITX2 Is elevated in *Mmp14* CKO tendons. A,** Q-PCR detection of *Pitx2* and **B**, *Plod2*
457 mRNA levels in control and *Mmp14* CKO tail tendons 5 weeks post tamoxifen treatment, at ZT3
458 and ZT15 (n=3). **C,** Per2::Luc iTTFs stably transduced with control or PITX22-GFP lentivirus (n=3),
459 demonstrating enhanced expression of *Pitx2* (n=9 and n=7; ****p<0.0001) and **D**, a concomitant
460 increase in *Plod2* mRNA expression (n=5; ***p<0.001). **E,** Live cell Airyscan imaging of Per2::Luc
461 iTTFs and *Mmp14* KO ITTFs stably transduced with Pitx2-GFP lentivirus. Cells were transiently
462 transduced with mCherry tagged MMP14 carrying a silent mutation in the CRISPR-Cas9 PAM site.
463 Pitx2-GFP was readily detected within the nucleus but also with punctate localisation within the
464 cell body in control cell, these correlated with regions also positive for MT1-MMP. Nuclear Pitx2-
465 GFP signals were stronger within *Mmp14* KO cells and also displayed reduced localisation within
466 the cell body. Re-expression of *Mmp14* within knockout cells reduced nuclear PITX2-GFP signals.
467 **F**, Quantification of mean nuclear GFP signal intensity (n=3; ****p<0.0001, **p<0.01). **G-J,** Q-PCR
468 demonstrating expression of *Mmp14* in PITX22-GFP expressing iTTFs, which resulted in reduced
469 *Pitx2* and *Plod2* mRNA expression, but enhanced *Col1a1* mRNA (n=3; **p<0.01).

470

471 **Figure 5. Recombinant MT1-MMP preferentially cleaves soluble collagen-I. A**, Fibril diameter
472 distribution of collagen fibrils dispersed from mouse Achilles tendons before treatment and 24 h
473 after treatment with and without rhMT1-MMP at 30 °C. *Effective hydrated fibril diameter (>500
474 fibrils measured). **B** Coomassie blue-stained gel showing incubation of monomeric and fibrillar
475 collagen-I with recombinant human MT1-MMP at 30 °C and 37 °C, in the presence or absence of
476 50 mM EDTA. M, monomeric; F, fibrillar collagen dispersed from Achilles tendon. rhMT1-MMP
477 generated ¾α1(I) and ¾α2(I) fragments from monomeric collagen I (red box) and from fibrillar
478 collagen (white box). Asterisk shows the b-crosslinked chains of collagen-I. A prominent faster
479 migrating b-dimer is seen in the MT1-MMP treated samples which occurs in the presence and
480 absence of 50 mM EDTA. **C**, Mass spectrum of rhMT1-MMP generated fragments from monomeric
481 collagen I shows the mass to charge ratio of individual ions resulting from MS/MS fragmentation

482 pattern between Gly_{775} and Ile_{776}. **D,** Precise fragmentation pattern that contributes to the
483 generation of b and y ions.

484

485 **Figure 6. Deletion of *Mmp14* weakens circadian entrainment. A**, Representative bioluminescence
486 recordings from Per2::Luc iTTFs (black) and single cell clones of CRISPR-Cas9 induced knockout of
487 *Mmp14* Per2::Luc fibroblasts (blue) after synchronization with dexamethasone. **B,**
488 Bioluminescence recordings from Per2::Luc iTTFs (grey) or *Mmp14* KO iTTFs (blue) that have been
489 transduced with a lentivirus expressing *Mmp14* (carrying a silent mutation in the CRISPR-Cas9
490 PAM site) from a CMV promoter (black and red). Restoration of *Mmp14* levels in *Mmp14* KO
491 fibroblasts reinstated dexamethasone induced circadian rhythms. **C**, Relative amplitude of control
492 iTTF cells, Clone #1 *Mmp14*-null iTTFs and Clone #1 *Mmp14*-null cells expressing *Mmp14* from a
493 CMV promoter (n=4).

494

495 **Supplementary information**

496 **Figure S1. *Mmp14* expression and MT1-MMP translation in tendon are under circadian clock**
497 **control. A,** Expression of *Mmp14* mRNA in WT mouse tail tendons analyzed by microarray every 4
498 h during 48 h, relative to the first time point. Three colored lines indicate the results from 3 probe
499 sets on the microarray chip, n=2; CT, circadian time (free-running time, in constant darkness). **B,**
500 Levels of MT1-MMP in WT mouse tail tendons analyzed by western blotting. Levels of GAPDH
501 protein served as a loading control. **C,** Relative expression of *Mmp14*, measured at zeitgeber time
502 3 (ZT3; 3 hours into the light phase) and ZT15 in mouse Achilles and tail tendons of WT mice (n=3
503 and **p=0.0045 for Achilles tendon; n=4 and **p=0.0093 for tail tendon), and **D,** tendon-specific
504 *Bmal1* knockout (*Scx-Cre::Bmal1*$^{lox/lox}$) mice (n=3 and p=0.6296 for Achilles tendon; n=3 and
505 p=0.7465 for tail tendon). **E,** Relative expression of *Mmp14*, measured at ZT3 and ZT15 in WT and
506 *ClockΔ19* tail tendons (n=3).

507

508 **Figure S2. *Mmp14*-deficient tendons accumulate small-diameter collagen fibrils.** Transmission
509 electron microscopy of control (**A**) and CKO (**B**) mouse tail tendons, at T4 (23 weeks postnatal age).
510 Scale bar, 0.5 µm. Asterisks indicate fibricarriers containing cross-sectional profiles of small-
511 diameter collagen fibrils.

512

513 **Figure S3. Depletion or inactivation of *Mmp14* weakens time-dependent differences of protein**
514 **abundance. A**, Correlation matrix showing Pearson's R-squared values between datasets resulting
515 from mass spectrometry analysis of tail tendon tissue from CKO and control mice at ZT3 and ZT15
516 time points within the circadian cycle (n=3 biological repeats; see Fig. 4). Greater similarity was
517 observed between samples at different timepoints than between CKO vs. Ctrl. **B,** Plot showing
518 fold-changes in protein abundance, correlating changes observed in *Mmp14* CKO tendon tissues
519 between ZT15 vs. ZT3 time points, to changes observed in control tissue between corresponding
520 time points. The data showed significant positive correlation, with a Pearson's R-squared value of
521 0.2421 ($p < 0.0001$). However, the difference between the ZT15 vs. ZT3 timepoints was
522 compressed in the *Mmp14* CKO tissues, evidenced by linear fit to the data (shown in red, with
523 gradient lower than y=x), and consistent with a dampened circadian response (n=3 biological
524 repeats).

525

526 **Figure S4. Interaction analysis of non-time-dependent matrisome proteins with differential**
527 **abundance in CKO tendons. A**, Map of reported interactions between some of the matrisome
528 proteins with increased abundance and **B**, decreased abundance in CKO tendons. MMP14 was
529 added to maps to indicate changes that may be directly influenced by *Mmp14* deletion. **C**, Relative
530 abundance of COL1A1 and COL1A2 peptides in control CKO tendons at ZT3 and ZT15.

531

532 **Figure S5. Transmission electron microscopy of *Col-r/r* mouse tendon. A**, schematic showing the
533 location of the ¾-¼ MMP cleavage site (arrow) in collagen-I and its absence in the *Col-r/r* mouse.
534 **B**, Electron microscopy images of tendons cross sections of 23 weeks old wild type and *Col-r/r*
535 mice. Scale bars, 0.5 µM. **C**, Fibril diameter distributions of fibrils measured in wild type and *Col-r/r*
536 tendons.

537

538 **Figure S6. MMP Inhibition and *Mmp14* weakens circadian entrainment. A**, Dose response curves
539 showing the effects of GM6001 on the viability of Per2::luc iTTFs assessed by Alamar blue. **B,**
540 Representative bioluminescence recordings from DMSO or GM6001 treated Per2::Luc iTTFs, with
541 and without synchronization with dexamethasone. **C**, *Mmp14* mRNA expression detected by Q-
542 PCR 72 hours after transfection of Per2::Luc iTTFs with scrambled (*siScram*) or *Mmp14* targeting
543 siRNA (*siMmp14*), (n=3). **D**, Representative bioluminescence recordings from *siScram* and

544 *siMmp14* transfected Per2::Luc fibroblasts, after synchronization with dexamethasone. **E**, Sanger
545 sequencing of *Mmp14* in iTTFs derived from the Per2::Luc mouse (control iTTFs) and a single cell
546 clone with *Mmp14* CRISPR-Cas9 knockout. Sequences proximal to the gRNA binding site are
547 shown. **F**, Western blot detection of MT1-MMP in control Per2::luc iTTFs and single cell clones of
548 *Mmp14* CRISPR-Cas9 knockouts.

549

550 **Movie 1:** Step-through movie generated from images collected by serial block face-scanning
551 electron microscopy of 23-week-old mouse Achilles tendon. The object in the center of the stack is
552 a cell with long outstretched processes surrounded by collagen fibrils oriented parallel to the long
553 axis of the tendon. Scale bar, 1 µm.

554

555 **Movie 2:** Step-through movie generated from images collected by serial block face-scanning
556 electron microscopy of 21-week-old (i.e., 13 weeks post tamoxifen treatment) conditional
557 knockout mouse Achilles tendon. Gross disruption of the tendon matrix has occurred with
558 collagen fibrils misaligned with respect to the tendon long axis and cell processes difficult to
559 identify. Scale bar, 1 µm.

560

561 **Table S1** is a list of proteins identified from control and *Mmp14* CKO tendons at ZT3 and ZT15 by
562 mass spectrometry. (XLSX)

563 **SourceData FS1** contains original blots for Fig. S1. (PDF)

564 **SourceData F5** contains original gels for Fig. 5. (PDF)

565

566 **Data availability**

567 Raw proteomic data was deposited to the ProteomeXchange Consortium via the PRIDE partner
568 repository with the data set identifier PXD031692.

569

570 **Experimental procedures**

571 **Mice.** The care and use of all mice in this study was carried out in accordance with the UK Home
572 Office regulations, UK Animals (Scientific Procedures) Act of 1986 under the Home Office licence

573 (70/8858) and with German legal guidelines. Ethical approval was granted by the University of
574 Manchester and by the Regierungspräsidium Köln, Germany (NRW authorization 50.203.2- K 37a,
575 20/05 and AZ2010.A342). The permission included the generation of CKO out animals. All mice
576 were housed in 12-h light/12-h dark cycle (LD) and are indicated where zeitgeber time (ZT) is used,
577 with the exception of wild type C57BL/6 mice housed in 12-h dark/12-h dark cycle (DD) that were
578 used for circadian time (CT) time-series microarray and protein extraction as previously described
579 [27]. To generate inducible CKO mice in which *Mmp14* is ablated in fibroblasts upon induction with
580 tamoxifen, we crossed mice expressing CreER recombinase under the control of the *Col1a2*
581 promoter (*Col1a2-CreERT2*; C57BL/6) [62] with C57BL/6 mice carrying the floxed exons (exons 2 to 4)
582 of the *Mmp14* gene [63] to produce *Col1a2-CreERT2::Mmp14*$^{lox/lox}$ CKO mice. To induce *Mmp14*
583 ablation, mice were fed tamoxifen-formulated chow at 5-weeks old for 4 weeks. To generate mice
584 in which *Bmal1* is ablated in tendon-lineage cells, we crossed mice expressing Cre recombinase
585 under the control of the *Scleraxis* promoter (*Scx-Cre*; C57BL/6) [64] with C57BL/6 mice carrying loxP
586 sites flanking the exon encoding the BMAL1 basic helix-loop-helix domain [65] bred on a background
587 with *PER2::Luciferase* knock-in [24] to produce *Scx-Cre::Bmal1*$^{lox/lox}$ KO mice. *Scx-Cre::Bmal1*$^{lox/lox}$ KO
588 mice were validated previously [5]. *ClockΔ19* mice were as described previously [66]. *Col1a1-r/r* mice
589 were imported from Jackson Laboratory (*B6;129S4-Col1a1*$^{tm1Jae/J}$) [36]. Mice that showed signs of
590 distress or had problems walking were humanely sacrificed using Home Office approved cervical
591 dislocation.

592

593 **Tissue culture.** Immortalized mouse tail tendon fibroblasts were prepared from Per2::Luc mice as
594 described previously [5]. To synchronize the internal circadian pacemaker, cells were treated with
595 100 nM dexamethasone as described previously [5]. +GM6001 treatment, cell viability

596

597 **Fusion protein constructs.** Lentivirus expression of *Mmp14* was achieved using vectors generated
598 by Vectorbuilder. Murine *Mmp14* coding sequences were expressed under a CMV promoter, with
599 mutation of the *Mmp14* targeting gRNA, AGATCAAGGCCAATGTTCGGAG, PAM site (AGG to AAA).
600 For mCherry tagging the mCherry coding sequence was introduced after amino acid 536 of murine
601 *Mmp14* following the design of Dr. Philippe Chavrier [67], these vectors also carried blasticidin
602 resistance gene. Pitx2-GFP expressing cells were cloned into pLenti PGK Neo DEST (Addgene
603 plasmid # 19067 ref[68]), EGFP was cloned at the C terminus of the coding sequence of Pitx2 isoform

604 1 (Origene; MR227617). Lentivirus particles were generated as previously described [69]. Stable cells
605 were created by neomycin selection (250 µg/mL) or 5 µg/mL blasticidin.

606

607 **CRISPR/Cas9.** To generate *Mmp14* knockout fibroblasts, immortalized tail tendon fibroblasts from
608 the Per2::Luc mouse, generated at previously described [70], were transduced with lentivirus
609 particles created from vectors co-expressing Cas9 and gRNA (ABMgood 302361140595). *Mmp14*
610 knockout were achieved using vectors encoding the gRNA AGATCAAGGCCAATGTTCGGAG. After
611 puromycin selection (2.5 µg/mL) we isolated single cell clones by FACS and confirmed knockout of
612 *Mmp14* by real-time PCR and western blotting.

613

614 **Bioluminescence imaging and recordings.** Bioluminescence was recorded as described previously
615 [5]. Briefly, tendon fibroblasts were cultured on 35 mm culture dish in recording media containing
616 0.1 mM luciferin (Merck) in the presence of 100 nM dexamethasone (Merck) and real-time
617 quantitative bioluminescence was recorded using lumiCycle apparatus (Actimetrics). Baseline
618 subtraction was carried out using a 24-hr moving average. Amplitude was calculated as peak-
619 trough difference in bioluminescence of the second peak using base-line subtracted data.

620

621 **Light microscopy.** Live cell super resolution microscopy for was performed using a Zeiss LSM 880
622 Axio Observer microscope with Airyscan detection system in SR mode using a Plan-Apochromat
623 63×/1.4 Oil DIC M27 objective (Carl Zeiss, Jena, Germany). Excitation was achieved using the
624 488 nm line from an argon laser and 594 nm HeNe laser and emitted light was collected through
625 appropriate filters to eliminate any spill-over. Raw images were Airyscan processed using the
626 default settings and analyzed using ZEN 2.1 software and the image brightness and contrast
627 adjusted using BestFit.

628

629 **RNA isolation and Q-PCR analysis.** RNA was isolated from Achilles and tail tendons as described
630 previously [71]. In brief, tissues were washed with ice-cold PBS 3 times and snap frozen in liquid
631 nitrogen with 500 µL TRIzol Reagent (Thermo Fisher Scientific) using a Mikro Dismembrator S (B.
632 Braun Biotech International) at 2000 Hz for 90 seconds two times. After, 500 µL TRIzol was added
633 to the homogenized samples and RNA was isolated according to the manufacturer's protocol.
634 DNase treatment of RNA was performed using RQ1 RNase-free DNase (Promega) according to

635 manufacturer's protocol. RNA integrity was assessed by gel electrophoresis and RNA
636 concentration was measured using a NanoDrop 2000 (Thermo Fisher Scientific). TaqMan Reverse
637 Transcription Reagents (Thermo Fisher Scientific) were used for complementary DNA synthesis
638 and SensiFAST SYBR kit reagents (Bioline) were used for Q-PCR. Primers sequences used were:
639 *Col1a1* GCC TGC TTC GTG TAA ACT CC and TTG GTT TTT GGT CAC GTT CA, *Mmp14* AGT GAC AGG
640 CAA GGC TGA TT and GCC CAC CTT AGG GGT GTA AT, *Pitx2* CCT TAC GGA AGC CCG AGT and AAA
641 GCC ATT CTT GCA CAG C, *Plod2* CAA ATC ATA AAA TCG TCT TTG CAG and CCT CTT CAG TGG GTC
642 GAT GT, and *Gapdh* AAC TTT GGC ATT GTG GAA GG and ACA CAT TGG GGG TAG GAA CA. The $2^{-\Delta\Delta Ct}$
643 method [72] was used to analyze relative fold changes in gene expression compared to the first time
644 point. Microarray data for *Mmp14* expression during 48 h was collected previously [27] and the data
645 is available on ArrayExpress (accession number E-MTAB-7743).

646

647 **Western blotting.** Protein purification and western blot analyses were performed as described
648 previously [5]. Wild type mice were kept in DD for 36 h to allow endogenous circadian rhythm of
649 gene expression. Protein was purified from tail tendons at 4-h intervals. Primary antibodies used
650 were mouse mAb to MT1-MMP (1:500; clone LEM-2/15.8, Millipore), mAb GAPDH (1:10000; clone
651 Gapdh71.1; Merck), and vinculin (1:500; clone hVIN-1, V9131).

652

653 **Sample preparation for proteomic analysis.** Tail tendons from wild type and *Mmp14* CKO mice
654 were collected at ZT3 and ZT15. Tissues were homogenized with a bullet blender (with 1.6 mm
655 steel beads; Next Advance) at maximum speed at 4 °C for 5 min in 200 µL of SL-DOC buffer (1.1%
656 sodium laurate, 0.3% sodium deoxycholate, 0.5 mM dithiothreitol (DTT) in 25 mM ammonium
657 bicarbonate), supplemented with protease and phosphatase inhibitor cocktails (Roche). Samples
658 were incubated at 4 °C for 5 min, alkylated with 12 µL of 30 mM of iodoacetamide for 20 min at
659 RT, followed by quenching with 12 µL of 30 mM DTT. Samples were centrifuged at maximum
660 speed for 10 min. Supernatants were transferred into LoBind tubes (Eppendorf) and protein
661 concentrations measured using a Millipore Direct Detect spectrometer. A total of 2 µg protein per
662 sample was digested using trypsin beads in accordance with the manufacturer's protocol (SMART
663 digestion kit, Thermo Scientific). Supernatants were extracted from the beads and 10% formic acid
664 added to adjust to pH 3. Samples were cleaned using an organic phase extraction method: 400 µL
665 ethylacetate (Sigma Aldrich) was added, the resulting solution thoroughly mixed, centrifuged, and
666 the organic phase extracted and discarded; this process was then repeated. Samples were then

667 desalted, in accordance with the manufacturer's protocol, using POROS R3 beads (Thermo Fisher)
668 and lyophilized in a speed-vac centrifuge (Heto).

669

670 **Liquid chromatography-coupled tandem mass spectrometry (LC-MS/MS).** Samples were
671 dissolved in 15 µl of 5% acetonitrile with 0.1% formic acid. Digested samples were analyzed using
672 an UltiMate® 3000 Rapid Separation liquid chromatography system (RSLC, Dionex Corporation)
673 coupled to either Q Exactive HF (Thermo Fisher Scientific) mass spectrometer. Peptides were
674 separated in a gradient of 95% A and 5% B to 7% B at 1 min, 18% B at 58 min, 27% B in 72 min and
675 60% B at 74 min at 300 nL/min using a 75 mm x 250 µm inner diameter 1.7 µM CSH C18, analytical
676 column (Waters). Peptides were selected for fragmentation automatically by data dependent
677 analysis.

678

679 **Proteomics data processing.** Spectra from multiple samples were aligned using Progenesis QI
680 (Nonlinear Dynamics) Peak-picking sensitivity was set to 4/5 and all other parameters were left as
681 defaults. Only peptides with charge between +1 to +4, with 2 or more isotopes were taken for
682 further analysis. Filtered peptides were identified using Mascot (Matrix Science UK), by searching
683 against the SwissProt and TREMBL mouse databases. The peptide database was modified to
684 search for alkylated cysteine residues (monoisotopic mass change, 57.021 Da), oxidized
685 methionine (15.995 Da), hydroxylation of asparagine, aspartic acid, proline or lysine (15.995 Da)
686 and phosphorylation of serine, tyrosine, threonine, histidine or aspartate (79.966 Da). A maximum
687 of 2 missed cleavages was allowed. Peptide detection intensities were exported from Progenesis
688 QI as Excel (Microsoft) spread sheets for further processing using code written in-house in
689 MATLAB with the bioinformatics toolbox (R2015a, The MathWorks, USA). Raw proteomic data was
690 deposited to the ProteomeXchange Consortium via the PRIDE partner repository with the data set
691 identifier PXD031692. Fold-change differences in the quantity of proteins detected in different
692 samples were calculated by fitting a linear regression model to take into account inter-sample
693 variation [73, 74]. Briefly, peptide intensities were logged and normalised by the median intensity;
694 protein fold-changes were calculated using a mixed-effects linear regression model, considering
695 random (peptides, biological replicates) and fixed (controlled variables) effects. Pathway
696 enrichment analysis was performed using the DAVID bioinformatics resource [75]. Peptide
697 identifications were filtered via Mascot scores so that only those with a Benjamini-Hochberg false
698 discovery rate (FDR) $\geq$ 0.05 remained. FDR filtering was performed on combined phospho-

699 enriched and non-enriched datasets as described in [76]. Raw ion intensities from peptides
700 belonging to proteins with fewer than 2 unique peptides (by sequence) per protein in the dataset
701 were excluded from quantification. Remaining intensities were logged and normalized by the
702 median logged peptide intensity. Peptides assigned to different isoforms were grouped into a
703 single "protein group" by gene name. Only peptides observed in at least 2 samples were used in
704 quantification. Missing values were assumed as missing due to low abundance, an assumption
705 others have shown is justified [77]. Imputation was performed at the peptide level following
706 normalization using a method similar to that employed by Perseus [78] whereby missing values were
707 imputed randomly from a normal distribution centered on the apparent limit of detection for this
708 experiment. The limit of detection in this instance was determined by taking the mean of all
709 minimum logged peptide intensities and down-shifting it by 1.6σ, where σ is the standard
710 deviation of minimum logged peptide intensities. The width of this normal distribution was set to
711 0.3σ as described in [78]. Fold-change differences in the quantity of proteins detected in different
712 time-points were calculated by fitting a mixed-effects linear regression model for each protein
713 with Huber weighting of residuals (doi: 10.1214/aoms/1177703732) as described in [77] using the
714 fitglme Matlab (The MathWorks, USA) function with the formula:

$$y_{iptb} = \beta_t + \beta_p + \beta_b$$

715 Where y_{ipt} represents the $\log_2$ (intensity) of peptide p belonging to protein i, at time-point t, in
716 batch b. βs represent effect sizes for the indicated coefficients. Peptide was entered as a random
717 effect whereas time-point was entered as a fixed effect. Standard error estimates were adjusted
718 with Empirical Bayes variance correction according to [79, 80]. Conditions were compared with
719 Student's t-tests with Benjamini-Hochberg correction for false positives (doi:10.1111/j.2517-
720 6161.1995.tb02031.x).

721

722 **Interactions analysis.** Protein interactions were mapped using Pathway Commons version 12 [81].

723

724 **Collagen content and crosslink analyses.** The hydroxylysine aldehyde (pyridinoline) cross-link
725 content of tendon samples was determined by HPLC after acid hydrolysis in 6 N HCl for 24 hrs at
726 108 °C as previously described [30]**.** Results were expressed in residues per mole of collagen based
727 on the hydroxyproline content assayed on the same hydrolysate as a measure of tissue collagen
728 content.

729

730 **Electron microscopy**

731 For transmission electron microscopy and morphometric analyses, tendons from mice were
732 prepared as described previously [29]. Fibril diameter, perimeter and area were measured using
733 ImageJ software to calculate circularity and fibril volume fraction as described previously [29]. Fibril
734 diameter distributions were plotted and fitted to 3-Gaussian distribution using Sigma Plot 12.0
735 software (Systat Software) as previously described [29]. For serial block face-scanning electron
736 microscopy (SBF-SEM), sample preparation and imaging was as described previously using an FEI
737 Quanta microscope fitted with a Gatan 3View® ultramicrotome [29]. Step-through image stacks were
738 generated using IMOD [82] and ImageJ [83].

739

740 **Recombinant MT1-MMP collagenase assay.** Cleanly dissected mouse Achilles tendons were snap
741 frozen in liquid nitrogen, and disrupted in 0.1 M Tris, pH 7.5 using a Mikro-dismembrator S (2 x 90
742 s, 2000 rpm, cooled with liquid nitrogen) to generate dispersed collagen fibrils. Recombinant
743 human MT1-MMP (250 µl) was dialyzed against four changes of assay buffer (50mM Tris-HCl, 150
744 mM NaCl, 10mM $CaCl_2$, 0.02% NaN_3, 0.05% Brij35, pH 7.5) at 0°C for 48 h. Pepsin-treated bovine
745 collagen type I (2 µg at 100 µg/ml final concentration; Thermo Fisher Scientific) or a mixture of
746 dispersed collagen fibrils from mouse Achilles tendon in assay buffer (50 mM Tris-HCl, 150 mM
747 NaCl, 10 mM CaCl2, 0.02% NaN3, 0.05% Brij35, pH 7.5) (2 µg at 200 µg/ml final concentration)
748 were incubated with or without rMT1-MMP in assay buffer (20 µl reactions) for 18 h at 30°C and
749 37°C. Protein concentrations of collagen substrates were confirmed by performing BCA protein
750 assay (ThermoFisher) according to manufacturer's instructions. Following digestion, samples were
751 separated by 10% SDS-PAGE for mass spectrometry analysis or sampled on a carbon-filmed 400
752 mesh copper grid for analysis by scanning transmission electron microscopy (STEM).

753

754 **Mass spectrometry.** Gels stained with Instant Blue stain for 1 h at room temperature. Gels were
755 de-stained in water. Proteins were excised from SDS-PAGE gels and dehydrated using acetonitrile
756 followed by vacuum centrifugation. Dried gel pieces were reduced with 10 mM dithiothreitol and
757 alkylated with 55 mM iodoacetamide. Gel pieces were then washed alternately with 25 mM
758 ammonium bicarbonate followed by acetonitrile and dried by vacuum centrifugation. Samples
759 were digested with trypsin, AspN or GluC overnight at 37°C, as above. Digested samples were

analyzed by LC-MS/MS using an UltiMate 3000 Rapid Separation LC (RSLC, Dionex Corporation, Sunnyvale, CA) coupled to an Orbitrap Elite (Thermo Fisher Scientific, Waltham, MA) mass spectrometer. Peptide mixtures were separated using a gradient from 92% A (0.1% FA in water) and 8% B (0.1% FA in acetonitrile) to 33% B, in 44 min at 300 nL/min, using a 250 mm x 75 µm i.d. 1.7 µM BEH C18, analytical column (Waters). Peptides were selected for fragmentation automatically by data dependent analysis.

STEM and measurement of fibril mass per unit length and calculation of effective hydrated fibril diameter. The mass per unit lengths of the unstained fibrils were measured using annular dark-field scanning transmission electron microscopy (STEM), as described [35]. STEM images were acquired on an FEI Tecnai 120 TEM (FEI, Eindhoven, Netherlands) fitted with STEM attachments, including a high-angle annular dark-field detector (Fischione, London, UK). A camera length of 350 cm was used to give an angular collection range of 15–75 mrad. Images (1024 x 1024) were acquired at an instrumental magnification of 17,000, corresponding to a pixel size of 5.23 nm, as determined using a diffraction grating replica (2160 lines per mm). Tobacco mosaic virus (a gift from Dr. John Carr, Department of Biochemistry, University of Cambridge, UK) was used as a calibration standard of mass per unit length (131 kDa nm^{-1}). The electron dose was kept sufficiently low (2–3 e A^{-2}) to produce negligible mass loss. Mass per unit length measurements were measured from STEM images using the Semper6 image analysis software (Synoptics, Cambridge, UK). For type I collagen fibrils the number (Na) of molecules in the transverse section of the overlap zone of each D-period is given by: $Na = M_L/(M/5D)$ where M_L is the mass per unit length of the fibril (kDa / nm), M is the molecular mass (kDa) and D is the axial periodicity (nm). Using values of M=290 kDa for type I collagen and D=67.2 nm (the measured axial periodicity of the unstained, dehydrated fibrils adsorbed on the carbon film) gives: $Na = 1.155 \times M_L$. Assuming a circular transverse shape for the fibril and a molecular packing density based on X-ray diffraction data from rat-tail tendon [84], the effective diameter (W_{eff}) of the fully hydrated fibril is then given by: $W_{eff} = 1.6 \sqrt{Na}$.

Statistical analysis. Data were evaluated using Two-tailed Student's t-test, two-way ANOVA or non-parametric, two-tailed Mann-Whitney test. Results were presented as mean ± SEM from at least three independent experiments. Differences were considered significant at the values of $*P < 0.05$, $**P < 0.01$ and $***P < 0.001$.

References

1. Canty, E.G. *et al.* Coalignment of plasma membrane channels and protrusions (fibripositors) specifies the parallelism of tendon. *The Journal of cell biology* **165**, 553-563 (2004).
2. Taylor, S.H. *et al.* Matrix metalloproteinase 14 is required for fibrous tissue expansion. *Elife* **4**, e09345 (2015).
3. Holmbeck, K. *et al.* MT1-MMP-deficient mice develop dwarfism, osteopenia, arthritis, and connective tissue disease due to inadequate collagen turnover. *Cell* **99**, 81-92 (1999).
4. Zhou, Z. *et al.* Impaired endochondral ossification and angiogenesis in mice deficient in membrane-type matrix metalloproteinase I. *Proc Natl Acad Sci U S A* **97**, 4052-4057 (2000).
5. Chang, J. *et al.* Circadian control of the secretory pathway maintains collagen homeostasis. *Nat Cell Biol* **22**, 74-86 (2020).
6. Sato, H. *et al.* A matrix metalloproteinase expressed on the surface of invasive tumour cells. *Nature* **370**, 61-65 (1994).
7. Tam, E.M., Morrison, C.J., Wu, Y.I., Stack, M.S. & Overall, C.M. Membrane protease proteomics: Isotope-coded affinity tag MS identification of undescribed MT1-matrix metalloproteinase substrates. *Proc Natl Acad Sci U S A* **101**, 6917-6922 (2004).
8. Hotary, K.B. *et al.* Membrane type I matrix metalloproteinase usurps tumor growth control imposed by the three-dimensional extracellular matrix. *Cell* **114**, 33-45 (2003).
9. Sodek, K.L., Ringuette, M.J. & Brown, T.J. MT1-MMP is the critical determinant of matrix degradation and invasion by ovarian cancer cells. *Br J Cancer* **97**, 358-367 (2007).
10. Ellerbroek, S.M., Wu, Y.I., Overall, C.M. & Stack, M.S. Functional interplay between type I collagen and cell surface matrix metalloproteinase activity. *J Biol Chem* **276**, 24833-24842 (2001).
11. Holmbeck, K., Bianco, P., Yamada, S. & Birkedal-Hansen, H. MT1-MMP: a tethered collagenase. *J Cell Physiol* **200**, 11-19 (2004).
12. Itoh, Y. Membrane-type matrix metalloproteinases: Their functions and regulations. *Matrix Biol* **44-46**, 207-223 (2015).
13. Tam, E.M., Wu, Y.I., Butler, G.S., Stack, M.S. & Overall, C.M. Collagen binding properties of the membrane type-1 matrix metalloproteinase (MT1-MMP) hemopexin C domain. The ectodomain of the 44-kDa autocatalytic product of MT1-MMP inhibits cell invasion by disrupting native type I collagen cleavage. *J Biol Chem* **277**, 39005-39014 (2002).
14. Hiraoka, N., Allen, E., Apel, I.J., Gyetko, M.R. & Weiss, S.J. Matrix metalloproteinases regulate neovascularization by acting as pericellular fibrinolysins. *Cell* **95**, 365-377 (1998).
15. Chun, T.H. *et al.* A pericellular collagenase directs the 3-dimensional development of white adipose tissue. *Cell* **125**, 577-591 (2006).
16. Shimizu-Hirota, R. *et al.* MT1-MMP regulates the PI3Kdelta.Mi-2/NuRD-dependent control of macrophage immune function. *Genes Dev* **26**, 395-413 (2012).
17. Mu, D. *et al.* The integrin alpha(v)beta8 mediates epithelial homeostasis through MT1-MMP-dependent activation of TGF-beta1. *J Cell Biol* **157**, 493-507 (2002).
18. Shi, F. & Sottile, J. MT1-MMP regulates the turnover and endocytosis of extracellular matrix fibronectin. *J Cell Sci* **124**, 4039-4050 (2011).
19. Roenneberg, T. & Merrow, M. Circadian clocks - the fall and rise of physiology. *Nat Rev Mol Cell Biol* **6**, 965-971 (2005).
20. Aggarwal, A. *et al.* The Circadian Clock Regulates Adipogenesis by a Per3 Crosstalk Pathway to Klf15. *Cell Rep* **21**, 2367-2375 (2017).
21. Keller, M. *et al.* A circadian clock in macrophages controls inflammatory immune responses. *Proc Natl Acad Sci U S A* **106**, 21407-21412 (2009).

22. Jensen, L.D. *et al.* Opposing effects of circadian clock genes bmal1 and period2 in regulation of VEGF-dependent angiogenesis in developing zebrafish. *Cell Rep* **2**, 231-241 (2012).
23. Yagita, K., Tamanini, F., van Der Horst, G.T. & Okamura, H. Molecular mechanisms of the biological clock in cultured fibroblasts. *Science* **292**, 278-281 (2001).
24. Yoo, S.H. *et al.* PERIOD2::LUCIFERASE real-time reporting of circadian dynamics reveals persistent circadian oscillations in mouse peripheral tissues. *Proceedings of the National Academy of Sciences of the United States of America* **101**, 5339-5346 (2004).
25. Takahashi, J.S. Transcriptional architecture of the mammalian circadian clock. *Nat Rev Genet* **18**, 164-179 (2017).
26. Pizarro, A., Hayer, K., Lahens, N.F. & Hogenesch, J.B. CircaDB: a database of mammalian circadian gene expression profiles. *Nucleic Acids Res* **41**, D1009-1013 (2013).
27. Yeung, C.Y. *et al.* Gremlin-2 is a BMP antagonist that is regulated by the circadian clock. *Sci Rep* **4**, 5183 (2014).
28. Zigrino, P. *et al.* Fibroblast-Derived MMP-14 Regulates Collagen Homeostasis in Adult Skin. *The Journal of investigative dermatology* **136**, 1575-1583 (2016).
29. Starborg, T. *et al.* Using transmission electron microscopy and 3View to determine collagen fibril size and three-dimensional organization. *Nat Protoc* **8**, 1433-1448 (2013).
30. Hudson, D.M. *et al.* Age-related type I collagen modifications reveal tissue-defining differences between ligament and tendon. *Matrix Biol Plus* **12**, 100070 (2021).
31. Ghosh, P., Saha, S.K., Nandi, S.S., Bhattacharya, S. & Roy, S.S. Involvement of Pitx2, a homeodomain transcription factor, in hypothyroidism associated reproductive disorders. *Cell Physiol Biochem* **20**, 887-898 (2007).
32. Hjalt, T.A., Amendt, B.A. & Murray, J.C. PITX2 regulates procollagen lysyl hydroxylase (PLOD) gene expression: implications for the pathology of Rieger syndrome. *J Cell Biol* **152**, 545-552 (2001).
33. Hendee, K.E. *et al.* PITX2 deficiency and associated human disease: insights from the zebrafish model. *Hum Mol Genet* **27**, 1675-1695 (2018).
34. Itoh, Y. *et al.* A common SNP risk variant MT1-MMP causative for Dupuytren's disease has a specific defect in collagenolytic activity. *Matrix Biol* **97**, 20-39 (2021).
35. Sherratt, M.J., Graham, H.K., Kielty, C.M. & Holmes, D.F. Mass-mapping of ECM macromolecules by scanning transmission electron microscopy. *Methods Mol Biol* **522**, 151-161 (2009).
36. Liu, X. *et al.* A targeted mutation at the known collagenase cleavage site in mouse type I collagen impairs tissue remodeling. *J Cell Biol* **130**, 227-237 (1995).
37. Wu, H. *et al.* Generation of collagenase-resistant collagen by site-directed mutagenesis of murine pro alpha 1(I) collagen gene. *Proc Natl Acad Sci U S A* **87**, 5888-5892 (1990).
38. Yamamoto, T. *et al.* Transcriptional oscillation of canonical clock genes in mouse peripheral tissues. *BMC Mol Biol* **5**, 18 (2004).
39. Ripperger, J.A. & Schibler, U. Rhythmic CLOCK-BMAL1 binding to multiple E-box motifs drives circadian Dbp transcription and chromatin transitions. *Nat Genet* **38**, 369-374 (2006).
40. Li, X. *et al.* CirGRDB: a database for the genome-wide deciphering circadian genes and regulators. *Nucleic Acids Res* **46**, D64-D70 (2018).
41. Yeung, C.C. *et al.* Circadian regulation of protein cargo in extracellular vesicles. *Sci Adv* **8**, eabc9061 (2022).
42. Schwanhausser, B. *et al.* Corrigendum: Global quantification of mammalian gene expression control. *Nature* **495**, 126-127 (2013).
43. Schwanhausser, B. *et al.* Global quantification of mammalian gene expression control. *Nature* **473**, 337-342 (2011).
44. Murchison, N.D. *et al.* Regulation of tendon differentiation by scleraxis distinguishes force-transmitting tendons from muscle-anchoring tendons. *Development* **134**, 2697-2708 (2007).
45. Kalson, N.S. *et al.* A structure-based extracellular matrix expansion mechanism of fibrous tissue growth. *Elife* **4** (2015).
46. Gumucio, J.P., Schonk, M.M., Kharaz, Y.A., Comerford, E. & Mendias, C.L. Scleraxis is required for the growth of adult tendons in response to mechanical loading. *JCI Insight* **5** (2020).

47. De Micheli, A.J. *et al.* Single-cell transcriptomic analysis identifies extensive heterogeneity in the cellular composition of mouse Achilles tendons. *Am J Physiol Cell Physiol* **319**, C885-C894 (2020).
48. Varcoe, T.J., Gatford, K.L. & Kennaway, D.J. Maternal circadian rhythms and the programming of adult health and disease. *Am J Physiol Regul Integr Comp Physiol* **314**, R231-R241 (2018).
49. Jobin, P.G., Butler, G.S. & Overall, C.M. New intracellular activities of matrix metalloproteinases shine in the moonlight. *Biochim Biophys Acta Mol Cell Res* **1864**, 2043-2055 (2017).
50. Young, B.B., Gordon, M.K. & Birk, D.E. Expression of type XIV collagen in developing chicken tendons: association with assembly and growth of collagen fibrils. *Dev Dyn* **217**, 430-439 (2000).
51. Ansorge, H.L. *et al.* Type XIV Collagen Regulates Fibrillogenesis: PREMATURE COLLAGEN FIBRIL GROWTH AND TISSUE DYSFUNCTION IN NULL MICE. *J Biol Chem* **284**, 8427-8438 (2009).
52. Vranka, J.A. *et al.* Prolyl 3-hydroxylase 1 null mice display abnormalities in fibrillar collagen-rich tissues such as tendons, skin, and bones. *J Biol Chem* **285**, 17253-17262 (2010).
53. Chin, J.R., Murphy, G. & Werb, Z. Stromelysin, a connective tissue-degrading metalloendopeptidase secreted by stimulated rabbit synovial fibroblasts in parallel with collagenase. Biosynthesis, isolation, characterization, and substrates. *J Biol Chem* **260**, 12367-12376 (1985).
54. Kalamajski, S. & Oldberg, A. Homologous sequence in lumican and fibromodulin leucine-rich repeat 5-7 competes for collagen binding. *J Biol Chem* **284**, 534-539 (2009).
55. Kalamajski, S. & Oldberg, A. The role of small leucine-rich proteoglycans in collagen fibrillogenesis. *Matrix Biol* **29**, 248-253 (2010).
56. Engebretsen, K.V. *et al.* Lumican is increased in experimental and clinical heart failure, and its production by cardiac fibroblasts is induced by mechanical and proinflammatory stimuli. *FEBS J* **280**, 2382-2398 (2013).
57. Mohammadzadeh, N. *et al.* The extracellular matrix proteoglycan lumican improves survival and counteracts cardiac dilatation and failure in mice subjected to pressure overload. *Sci Rep* **9**, 9206 (2019).
58. Jobin, P.G. *et al.* Moonlighting matrix metalloproteinase substrates: Enhancement of proinflammatory functions of extracellular tyrosyl-tRNA synthetase upon cleavage. *J Biol Chem* **295**, 2186-2202 (2020).
59. Attur, M. *et al.* Membrane-type 1 Matrix Metalloproteinase Modulates Tissue Homeostasis by a Non-proteolytic Mechanism. *iScience* **23**, 101789 (2020).
60. Maybee, D.V., Ink, N.L. & Ali, M.A.M. Novel Roles of MT1-MMP and MMP-2: Beyond the Extracellular Milieu. *Int J Mol Sci* **23** (2022).
61. Ip, Y.C., Cheung, S.T. & Fan, S.T. Atypical localization of membrane type 1-matrix metalloproteinase in the nucleus is associated with aggressive features of hepatocellular carcinoma. *Mol Carcinog* **46**, 225-230 (2007).
62. Zheng, B., Zhang, Z., Black, C.M., de Crombrugghe, B. & Denton, C.P. Ligand-dependent genetic recombination in fibroblasts : a potentially powerful technique for investigating gene function in fibrosis. *Am J Pathol* **160**, 1609-1617 (2002).
63. Zigrino, P. *et al.* Loss of epidermal MMP-14 expression interferes with angiogenesis but not with re-epithelialization. *Eur J Cell Biol* **91**, 748-756 (2012).
64. Blitz, E., Sharir, A., Akiyama, H. & Zelzer, E. Tendon-bone attachment unit is formed modularly by a distinct pool of Scx- and Sox9-positive progenitors. *Development* **140**, 2680-2690 (2013).
65. Storch, K.F. *et al.* Intrinsic circadian clock of the mammalian retina: importance for retinal processing of visual information. *Cell* **130**, 730-741 (2007).
66. Vitaterna, M.H. *et al.* Mutagenesis and mapping of a mouse gene, Clock, essential for circadian behavior. *Science* **264**, 719-725 (1994).
67. Rosse, C. *et al.* Control of MT1-MMP transport by atypical PKC during breast-cancer progression. *Proc Natl Acad Sci U S A* **111**, E1872-1879 (2014).
68. Campeau, E. *et al.* A versatile viral system for expression and depletion of proteins in mammalian cells. *PLoS One* **4**, e6529 (2009).

69. Calverley, B.C., Kadler, K.E. & Pickard, A. Dynamic High-Sensitivity Quantitation of Procollagen-I by Endogenous CRISPR-Cas9 NanoLuciferase Tagging. *Cells* **9** (2020).
70. Pickard, A. *et al.* Preservation of circadian rhythms by the protein folding chaperone, BiP. *FASEB journal : official publication of the Federation of American Societies for Experimental Biology* **33**, 7479-7489 (2019).
71. Yeung, C.Y. *et al.* Chick tendon fibroblast transcriptome and shape depend on whether the cell has made its own collagen matrix. *Scientific reports* **5**, 13555 (2015).
72. Livak, K.J. & Schmittgen, T.D. Analysis of relative gene expression data using real-time quantitative PCR and the 2(-Delta Delta C(T)) Method. *Methods* **25**, 402-408 (2001).
73. Mallikarjun, V., Richardson, S.M. & Swift, J. BayesENproteomics: Bayesian Elastic Nets for Quantification of Peptidoforms in Complex Samples. *J Proteome Res* **19**, 2167-2184 (2020).
74. Gilbert, H.T.J. *et al.* Nuclear decoupling is part of a rapid protein-level cellular response to high-intensity mechanical loading. *Nat Commun* **10**, 4149 (2019).
75. Huang da, W., Sherman, B.T. & Lempicki, R.A. Systematic and integrative analysis of large gene lists using DAVID bioinformatics resources. *Nat Protoc* **4**, 44-57 (2009).
76. Bekker-Jensen, D.B. *et al.* An Optimized Shotgun Strategy for the Rapid Generation of Comprehensive Human Proteomes. *Cell Syst* **4**, 587-599 e584 (2017).
77. Goeminne, L.J., Gevaert, K. & Clement, L. Peptide-level Robust Ridge Regression Improves Estimation, Sensitivity, and Specificity in Data-dependent Quantitative Label-free Shotgun Proteomics. *Mol Cell Proteomics* **15**, 657-668 (2016).
78. Tyanova, S., Temu, T. & Cox, J. The MaxQuant computational platform for mass spectrometry-based shotgun proteomics. *Nat Protoc* **11**, 2301-2319 (2016).
79. Smyth, G.K. Linear models and empirical bayes methods for assessing differential expression in microarray experiments. *Stat Appl Genet Mol Biol* **3**, Article3 (2004).
80. Kammers, K., Cole, R.N., Tiengwe, C. & Ruczinski, I. Detecting Significant Changes in Protein Abundance. *EuPA Open Proteom* **7**, 11-19 (2015).
81. Rodchenkov, I. *et al.* Pathway Commons 2019 Update: integration, analysis and exploration of pathway data. *Nucleic Acids Res* **48**, D489-D497 (2020).
82. Kremer, J.R., Mastronarde, D.N. & McIntosh, J.R. Computer visualization of three-dimensional image data using IMOD. *J Struct Biol* **116**, 71-76 (1996).
83. Schneider, C.A., Rasband, W.S. & Eliceiri, K.W. NIH Image to ImageJ: 25 years of image analysis. *Nat Methods* **9**, 671-675 (2012).
84. Holmes, D.F., Graham, H.K., Trotter, J.A. & Kadler, K.E. STEM/TEM studies of collagen fibril assembly. *Micron* **32**, 273-285 (2001).

Figure 1

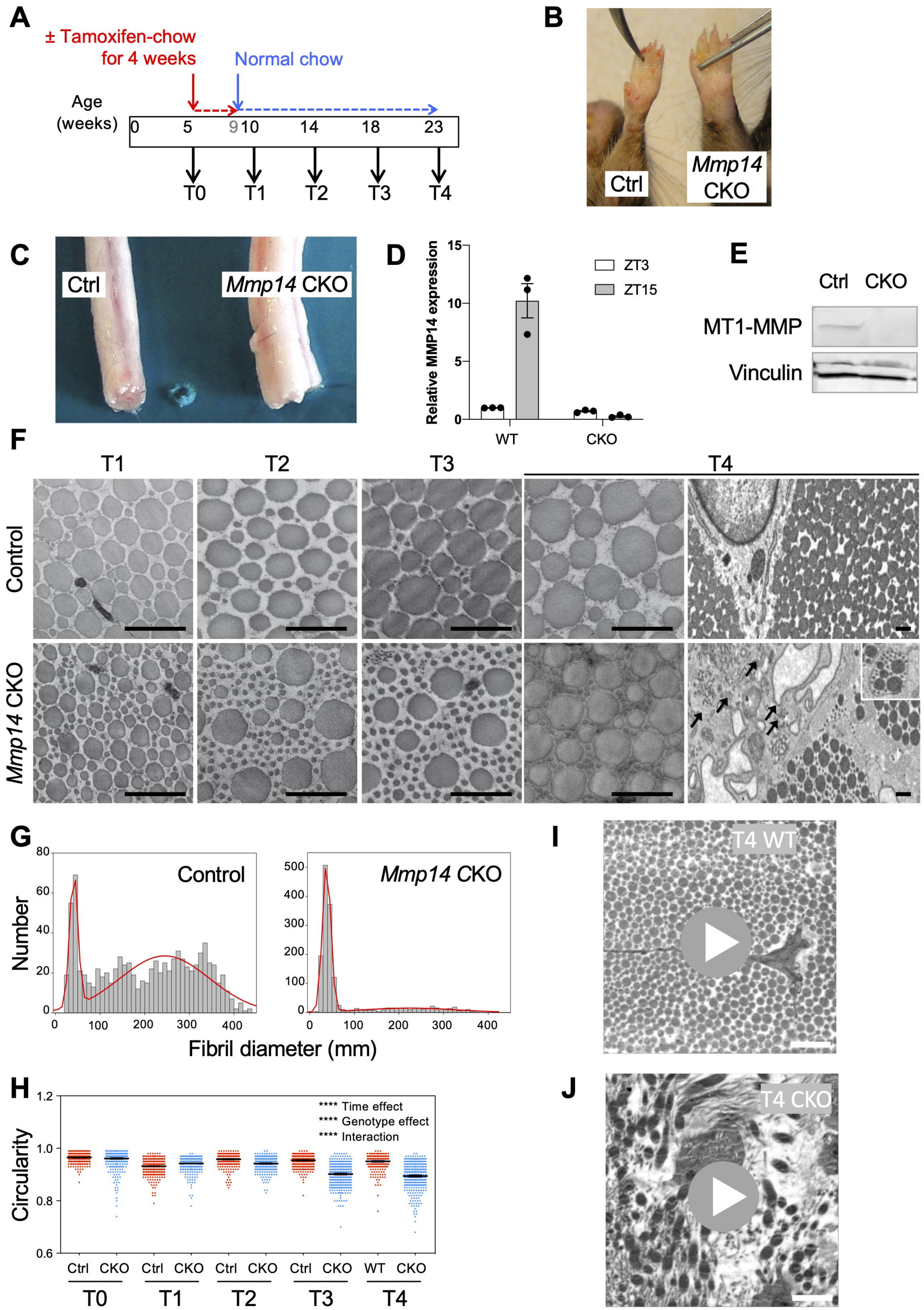
A
± Tamoxifen-chow
for 4 weeks
Normal chow
Age
(weeks)
0
5
9
10
14
18
23
T0
T1
T2
T3
T4
B
Ctrl
Mmp14
CKO
C
Ctrl
Mmp14 CKO
D
Relative MMP14 expression
15
10
5
0
ZT3
ZT15
WT
CKO
E
Ctrl
CKO
MT1-MMP
Vinculin
F
T1
T2
T3
T4
Control
Mmp14 CKO
G
Control
Mmp14 CKO
Number
80
60
40
20
0
500
400
300
200
100
0
100
200
300
400
Fibril diameter (mm)
H
Circularity
1.2
1.0
0.8
0.6
**** Time effect
**** Genotype effect
**** Interaction
Ctrl
CKO
Ctrl
CKO
Ctrl
CKO
Ctrl
CKO
WT
CKO
T0
T1
T2
T3
T4
I
T4 WT
J
T4 CKO

Figure 2

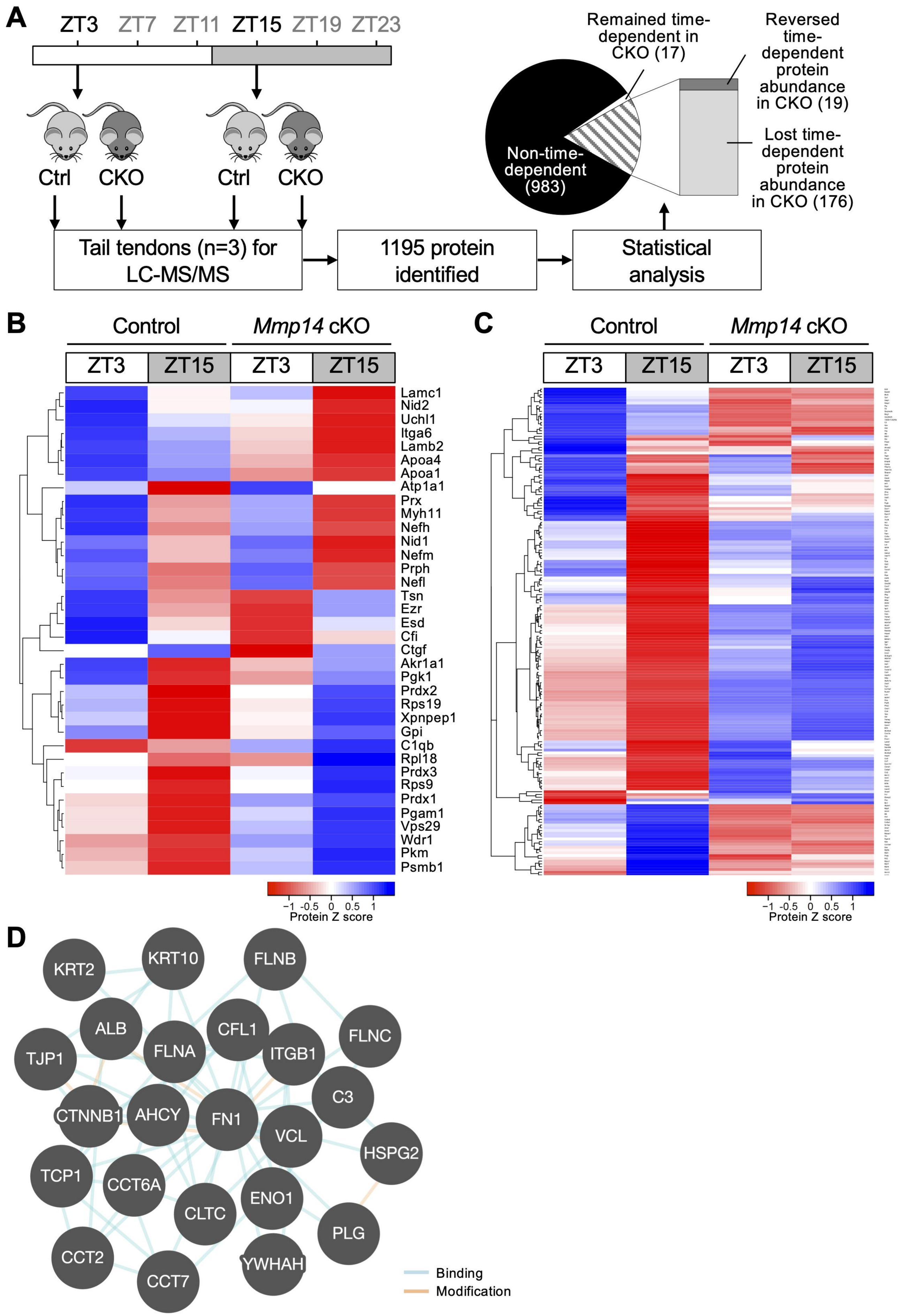
A
ZT3 ZT7 ZT11 ZT15 ZT19 ZT23
Ctrl CKO Ctrl CKO
Tail tendons (n=3) for LC-MS/MS
1195 protein identified
Statistical analysis
Remained time-dependent in CKO (17)
Reversed time-dependent protein abundance in CKO (19)
Lost time-dependent protein abundance in CKO (176)
Non-time-dependent (983)
B
Control
Mmp14 cKO
ZT3 ZT15 ZT3 ZT15
Lamc1
Nid2
Uchl1
Itga6
Lamb2
Apoa4
Apoa1
Atp1a1
Prx
Myh11
Nefh
Nid1
Nefm
Prph
Nefl
Tsn
Ezr
Esd
Cfi
Ctgf
Akr1a1
Pgk1
Prdx2
Rps19
Xpnpep1
Gpi
C1qb
Rpl18
Prdx3
Rps9
Prdx1
Pgam1
Vps29
Wdr1
Pkm
Psmb1
−1 -0.5 0 0.5 1
Protein Z score
C
Control
Mmp14 cKO
ZT3 ZT15 ZT3 ZT15
−1 -0.5 0 0.5 1
Protein Z score
D
KRT2
KRT10
FLNB
ALB
CFL1
FLNC
TJP1
FLNA
ITGB1
C3
CTNNB1
AHCY
FN1
VCL
HSPG2
TCP1
CCT6A
ENO1
CLTC
PLG
CCT2
YWHAH
CCT7
Binding
Modification

Figure 3

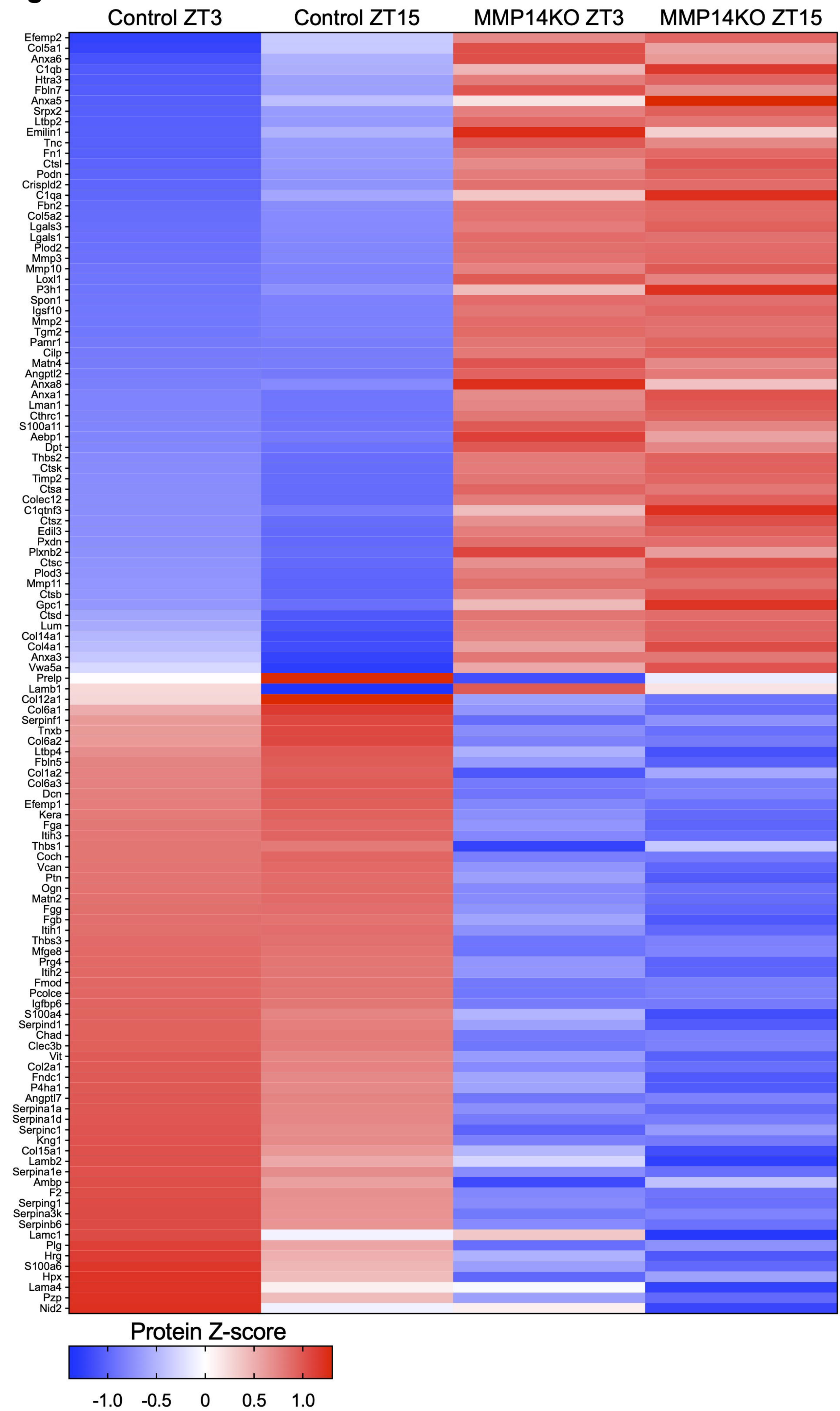
Control ZT3
Control ZT15
MMP14KO ZT3
MMP14KO ZT15
Efemp2
Col5a1
Anxa6
C1qb
Htra3
Fbln7
Anxa5
Srpx2
Ltbp2
Emilin1
Tnc
Fn1
Ctsl
Podn
Crispld2
C1qa
Fbn2
Col5a2
Lgals3
Lgals1
Plod2
Mmp3
Mmp10
Loxl1
P3h1
Spon1
Igsf10
Mmp2
Tgm2
Pamr1
Cilp
Matn4
Angptl2
Anxa8
Anxa1
Lman1
Cthrc1
S100a11
Aebp1
Dpt
Thbs2
Ctsk
Timp2
Ctsa
Colec12
C1qtnf3
Ctsz
Edil3
Pxdn
Plxnb2
Ctsc
Plod3
Mmp11
Ctsb
Gpc1
Ctsd
Lum
Col14a1
Col4a1
Anxa3
Vwa5a
Prelp
Lamb1
Col12a1
Col6a1
Serpinf1
Tnxb
Col6a2
Ltbp4
Fbln5
Col1a2
Col6a3
Dcn
Efemp1
Kera
Fga
Itih3
Thbs1
Coch
Vcan
Ptn
Ogn
Matn2
Fgg
Fgb
Itih1
Thbs3
Mfge8
Prg4
Itih2
Fmod
Pcolce
Igfbp6
S100a4
Serpind1
Chad
Clec3b
Vit
Col2a1
Fndc1
P4ha1
Angptl7
Serpina1a
Serpina1d
Serpinc1
Kng1
Col15a1
Lamb2
Serpina1e
Ambp
F2
Serping1
Serpina3k
Serpinb6
Lamc1
Plg
Hrg
S100a6
Hpx
Lama4
Pzp
Nid2
Protein Z-score
-1.0
-0.5
0
0.5
1.0

Figure 4

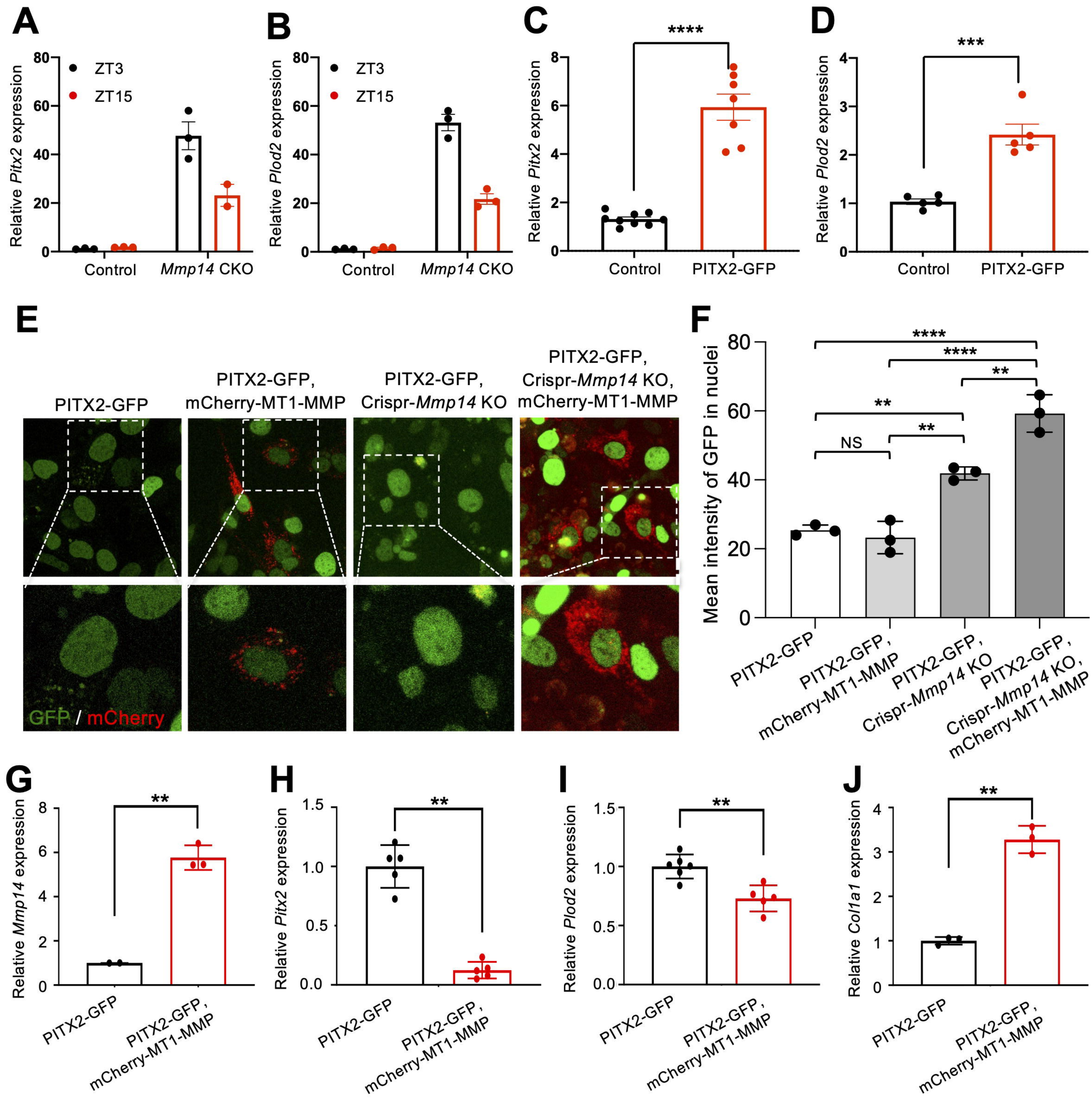
A
Relative Pitx2 expression
ZT3
ZT15
Control
Mmp14 CKO
B
Relative Plod2 expression
ZT3
ZT15
Control
Mmp14 CKO
C
Relative Pitx2 expression
****
Control
PITX2-GFP
D
Relative Plod2 expression
***
Control
PITX2-GFP
E
PITX2-GFP
PITX2-GFP, mCherry-MT1-MMP
PITX2-GFP, Crispr-Mmp14 KO
PITX2-GFP, Crispr-Mmp14 KO, mCherry-MT1-MMP
GFP / mCherry
F
Mean intensity of GFP in nuclei
****
****
**
**
**
NS
PITX2-GFP
PITX2-GFP, mCherry-MT1-MMP
PITX2-GFP, Crispr-Mmp14 KO
PITX2-GFP, Crispr-Mmp14 KO, mCherry-MT1-MMP
G
Relative Mmp14 expression
**
PITX2-GFP
PITX2-GFP, mCherry-MT1-MMP
H
Relative Pitx2 expression
**
PITX2-GFP
PITX2-GFP, mCherry-MT1-MMP
I
Relative Plod2 expression
**
PITX2-GFP
PITX2-GFP, mCherry-MT1-MMP
J
Relative Col1a1 expression
**
PITX2-GFP
PITX2-GFP, mCherry-MT1-MMP

Figure 5

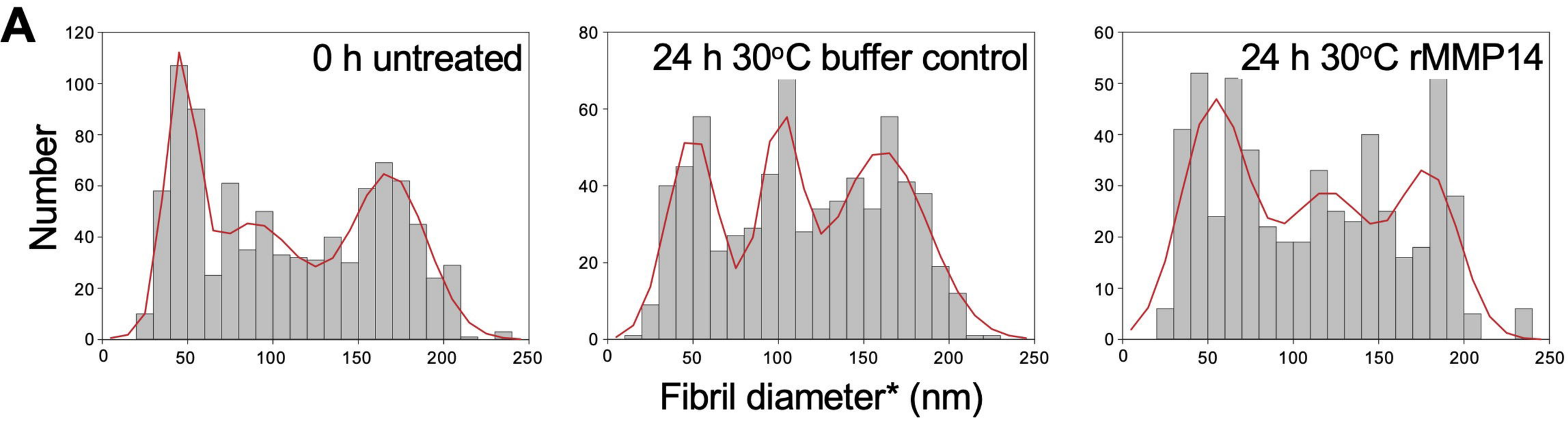
A
0 h untreated
24 h 30°C buffer control
24 h 30°C rMMP14
Number
Fibril diameter* (nm)

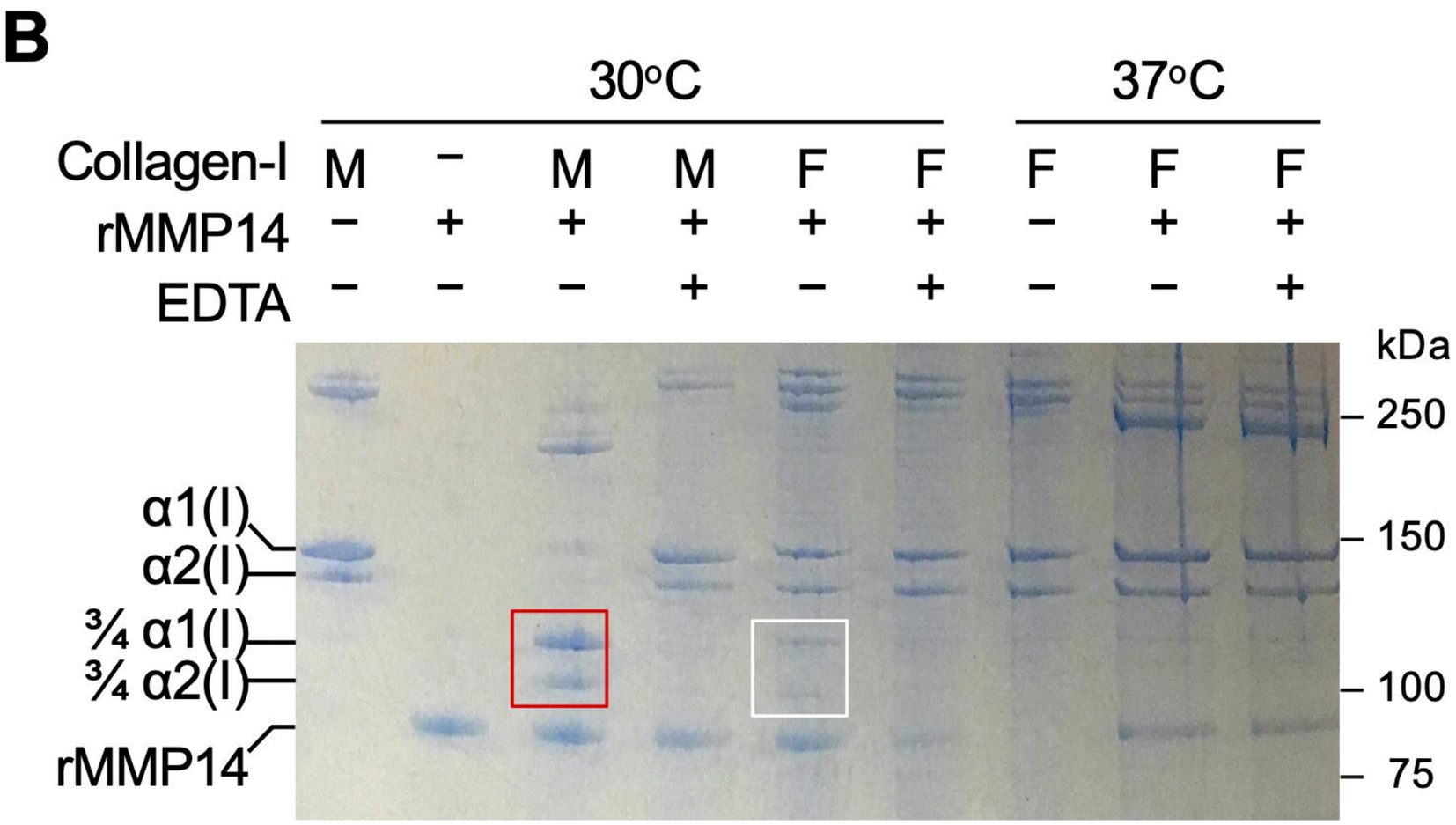
B
30°C
37°C
Collagen-I M − M M F F F F F
rMMP14 − + + + + + − + +
EDTA − − − + − + − − +
kDa
250
150
100
75
α1(I)
α2(I)
¾ α1(I)
¾ α2(I)
rMMP14

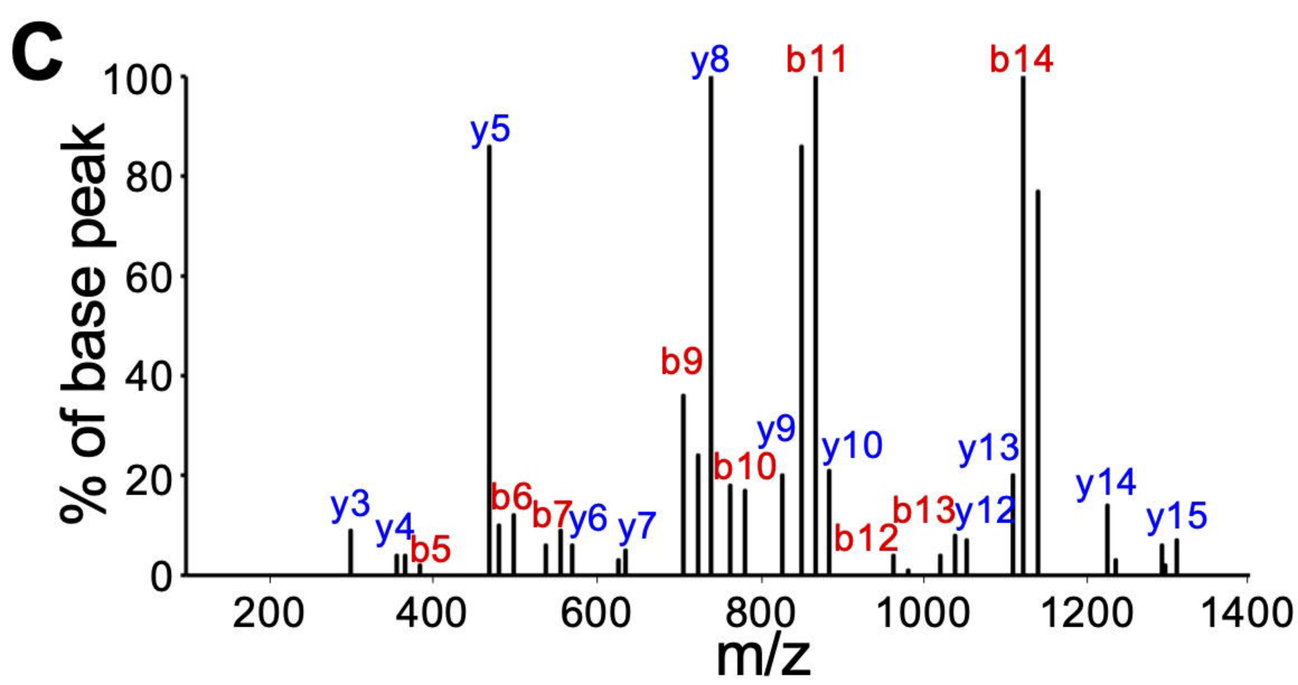
C
% of base peak
m/z
y3 y4 b5 y5 b6 b7 y6 y7 b9 y8 b10 y9 b11 b12 y10 b13 y12 y13 b14 y14 y15

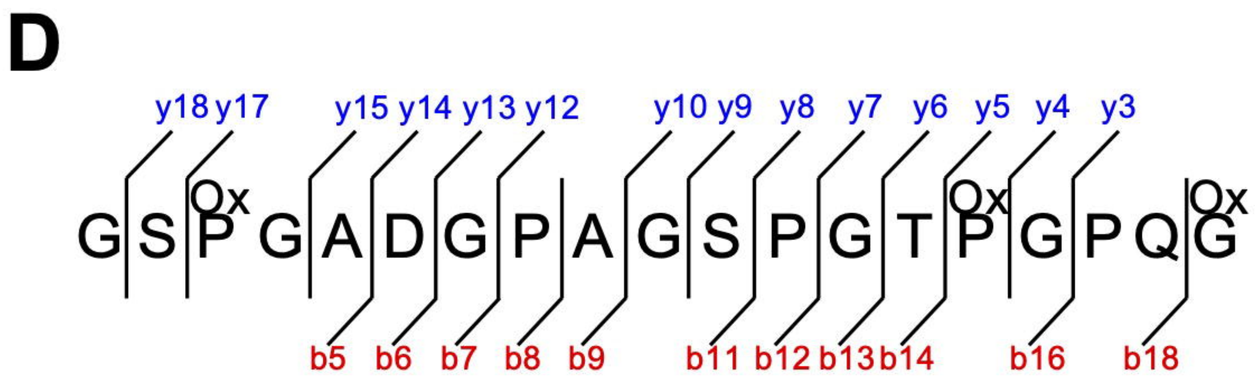
D
y18 y17 y15 y14 y13 y12 y10 y9 y8 y7 y6 y5 y4 y3
G S P G A D G P A G S P G T P G P Q G
Ox Ox Ox
b5 b6 b7 b8 b9 b11 b12 b13 b14 b16 b18

Figure 6

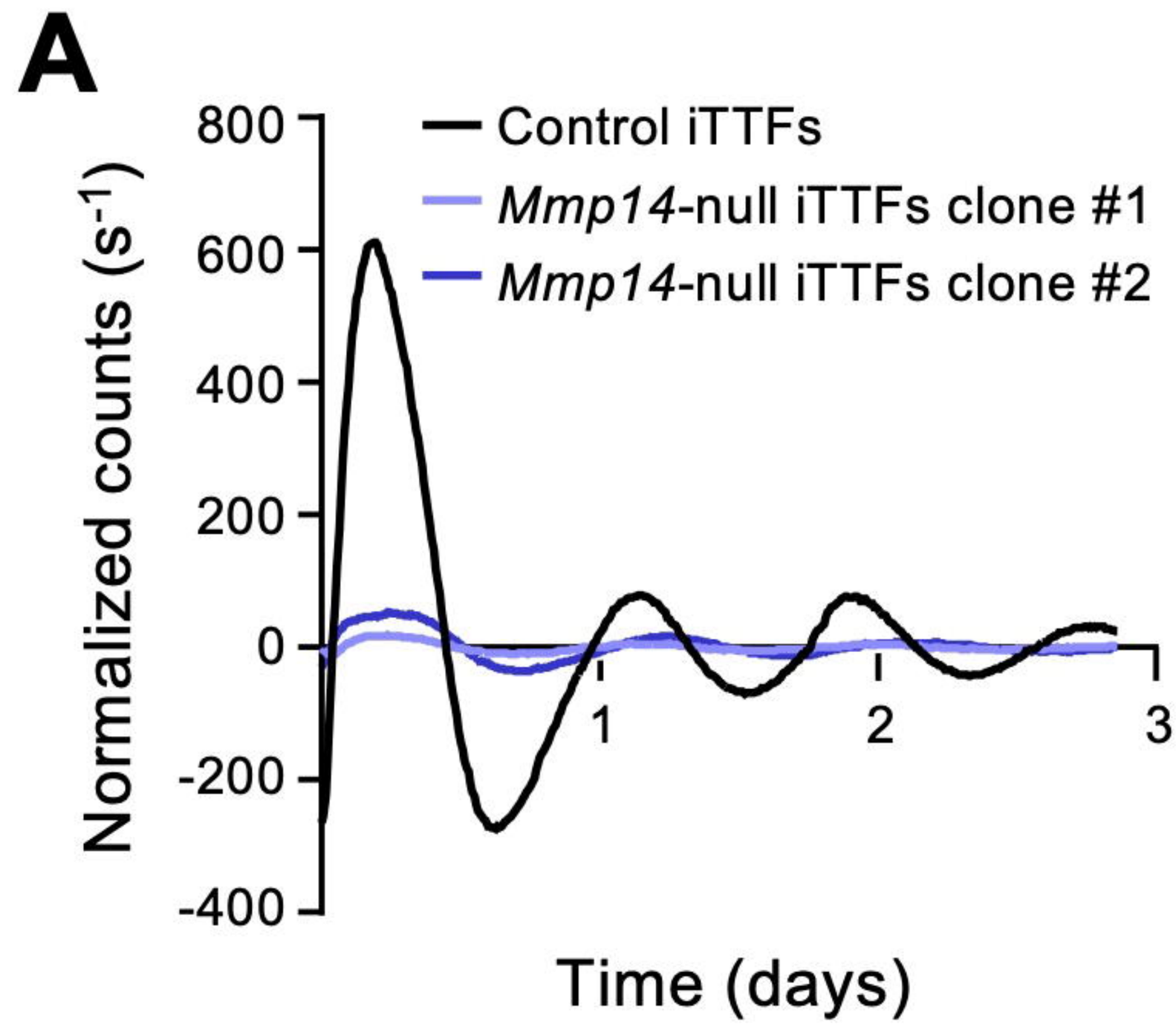
A
Control iTTFs
Mmp14-null iTTFs clone #1
Mmp14-null iTTFs clone #2
Normalized counts (s-1)
800
600
400
200
0
-200
-400
1
2
3
Time (days)

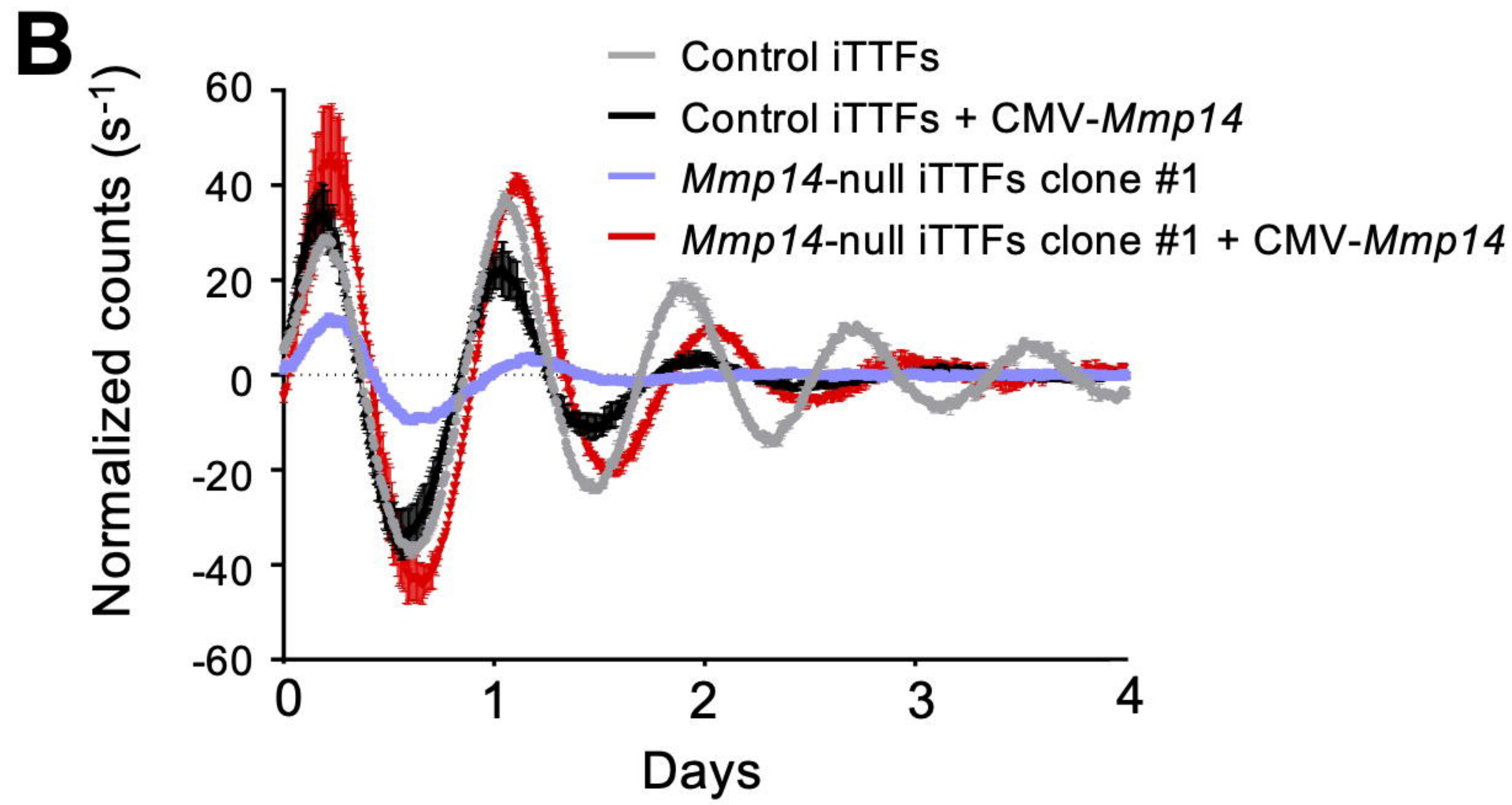
B
Control iTTFs
Control iTTFs + CMV-Mmp14
Mmp14-null iTTFs clone #1
Mmp14-null iTTFs clone #1 + CMV-Mmp14
Normalized counts (s-1)
60
40
20
0
-20
-40
-60
0
1
2
3
4
Days

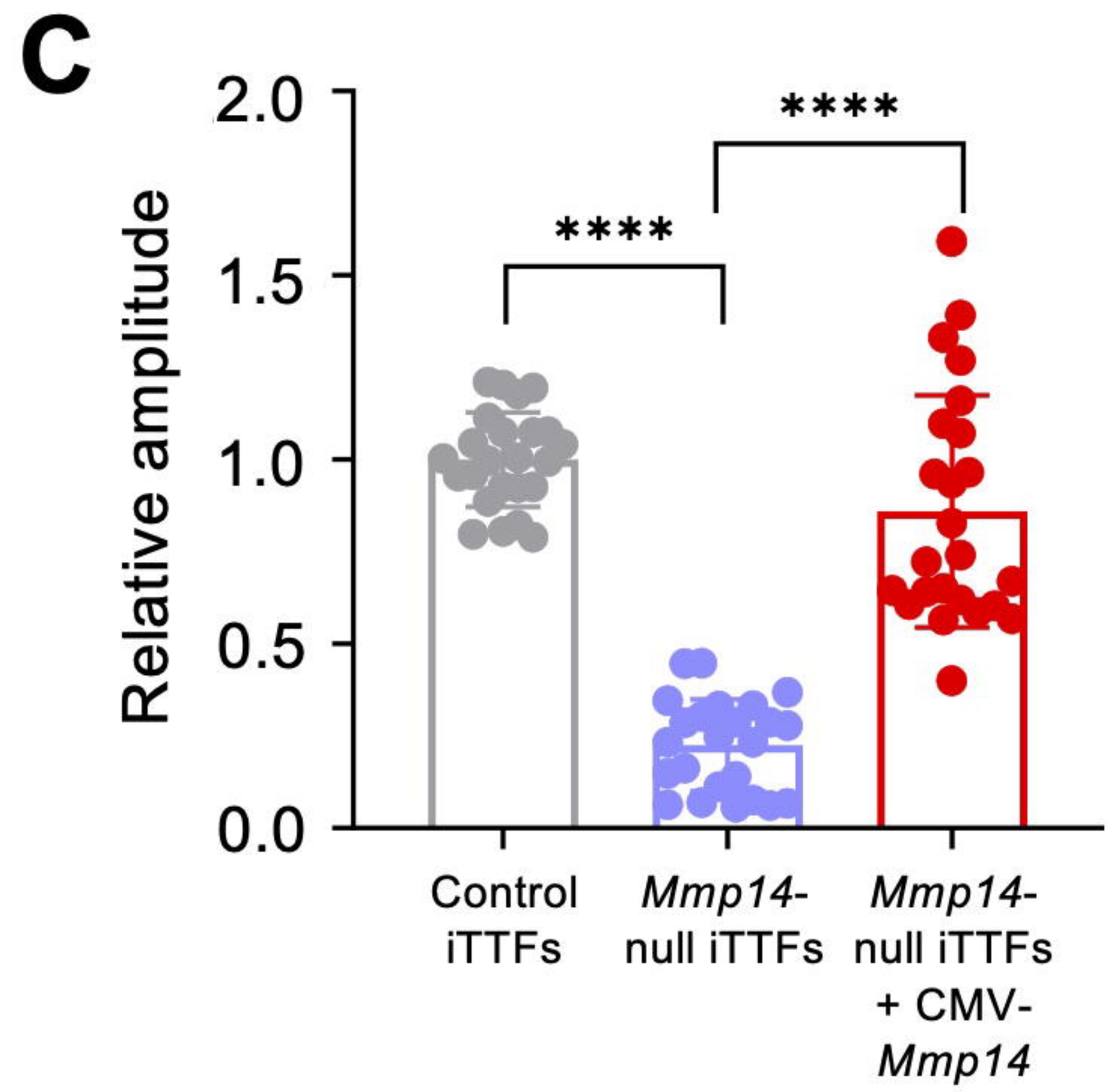
C
Relative amplitude
2.0
1.5
1.0
0.5
0.0
****
****
Control iTTFs
Mmp14-null iTTFs
Mmp14-null iTTFs + CMV-Mmp14